Figure 4. Zfp277 is required for the re-localization of PRC1, but not PRC2. A. A schematic representation of the *Ink4a/Arf* locus in MEFs. ChIP assays were performed using anti-Bmi1, Ring1B, Mel18, H2AK119ub1, Ezh2, Jmjd3, and H3K27me3 antibodies. Regions amplified from the precipitated DNA by site-specific quantitative PCR are indicated by arrows. **B–H.** Q-ChIP analysis of the $p19^{Arf}$ exon 1b and $p16^{Ink4a}$ exon 1a. Wild-type MEFs and $Zfp277^{-/-}$ MEFs at passage 2 with or without NAC treatment were subjected to ChIP analyses using the indicated antibodies. Percentages of input DNA are shown as the mean ± S.D. for multiple experiments (n>6). Statistical significance was determined with Student's t-test; $^{**}p<0.01$, $^{***}p<0.001$.
doi:10.1371/journal.pone.0012373.g004

oxidative stress. The generation or scavenging of ROS leads to the eviction or restoration of Zfp277 and PcG proteins at the *Ink4a/Arf* locus. In this cycle, Zfp277 plays an essential role in the re-localization of PRC1 but not PRC2 (Figure 7D).

NAC treatment of both $Zfp277^{-/-}$ and $Bmi1^{-/-}$ MEFs restored the binding of only PRC2, not PRC1, to the *Ink4a/Arf* locus. Nonetheless, it efficiently achieved a repressive state at the *Ink4a/Arf* locus and overrode the limited replicative life span of MEFs. Of importance, our ChIP analysis showed that neither Zfp277 nor Bmi1-deficiency affected the distribution of Mel18 at the *Ink4a/Arf* locus in the presence of NAC, suggesting that Mel18 is recruited to the *Ink4a/Arf* locus independently of Zfp277 or Bmi1. It is reported that human MEL18 forms a BMI1-independent PRC1 complex with RNF2, exhibiting E3 ubiquitin ligase activity for histone H2A [37]. Mel18 and Bmi1 knockout mice showed similar phenotypes at least for cell proliferation [15,52] and the knockout of both genes revealed that they synergistically maintain Hox gene expression during development

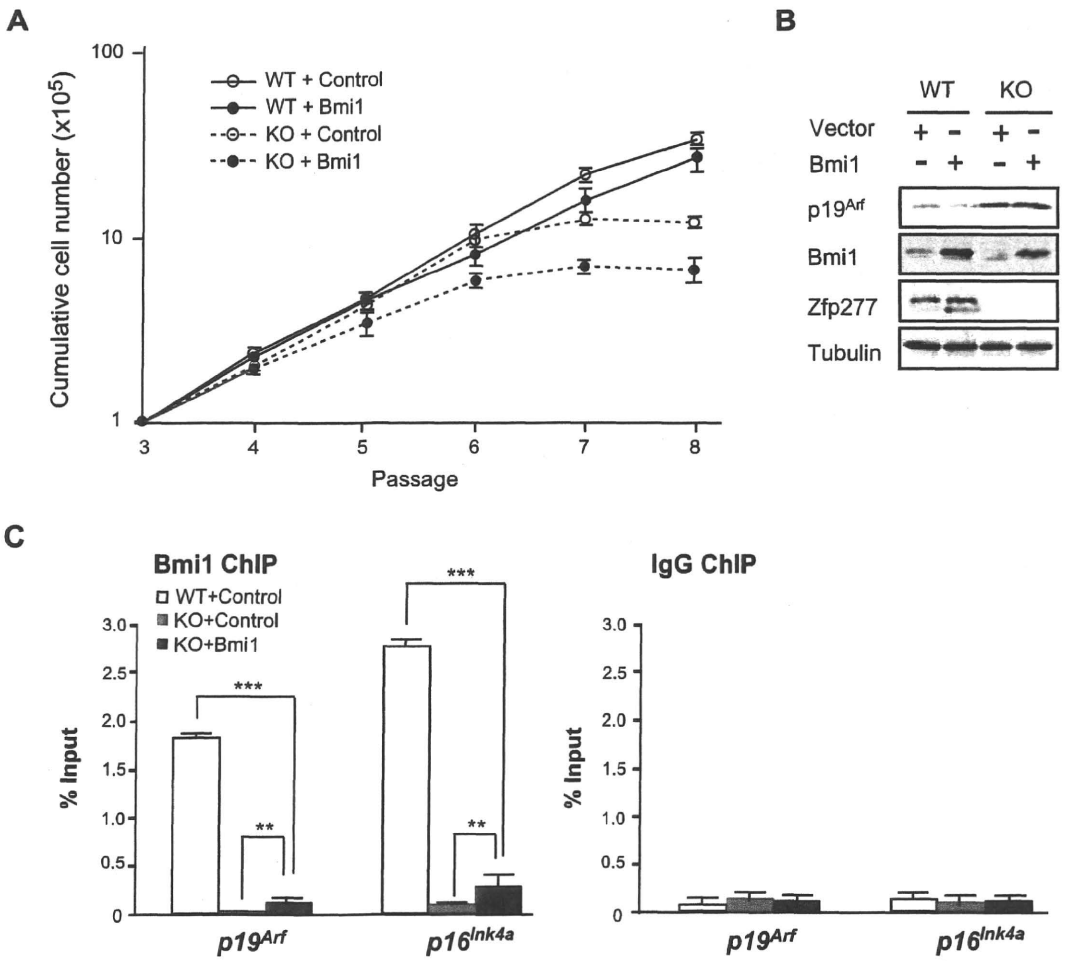

Figure 5. Forced expression of Bmi1 does not repress the *Ink4a-Arf* genes in $Zfp277^{-/-}$ MEFs. A. Bmi1 does not rescue $Zfp277^{-/-}$ MEFs from premature senescence. Wild-type and $Zfp277^{-/-}$ MEFs were transduced with either a control or a *Bmi1* retrovirus and cell growth was monitored every three days by replating at 1×10^5 cells/plate. Cumulative cell numbers are shown as the mean ± SD for three independent triplicate experiments. **B.** Bmi1 does not repress the *Ink4a-Arf* genes in $Zfp277^{-/-}$ MEFs. Wild-type and $Zfp277^{-/-}$ MEFs were transduced with either a control or a *Bmi1* retrovirus and the expression of $p19^{Arf}$ was detected by Western blot analysis. Tubulin was used as a loading control. **C.** ChIP analysis of Bmi1 in Bmi1-transduced $Zfp277^{-/-}$ MEFs. $Zfp277^{-/-}$ MEFs transduced with either a control or a *Bmi1* retrovirus were subjected to ChIP analyses using an anti-Bmi1 antibody and control IgG. The ChIP analysis of Bmi1 in wild-type MEFs at passage 2 is shown as a control. Percentages of input DNA are shown as the mean ± S.D. for three independent experiments. Statistical significance was determined with Student's t-test; $^{**}p<0.01$, $^{***}p<0.001$.
doi:10.1371/journal.pone.0012373.g005

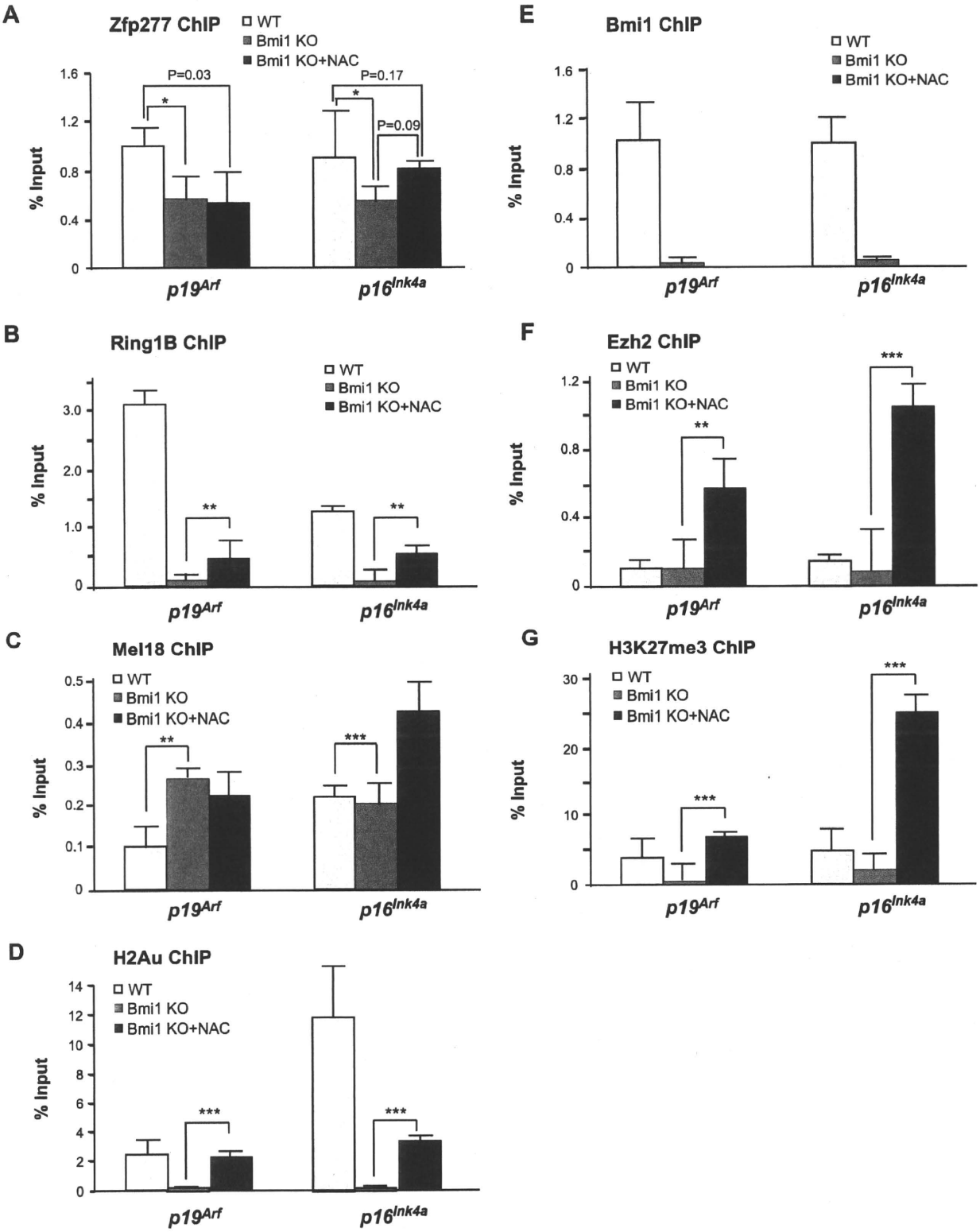

Figure 6. *Bmi1*-deficiency does not greatly affect the binding of Zfp277 to the *Ink4a/Arf* locus in early passage presenescent cells. A–G. The ChIP analysis of the $p19^{Arf}$ exon 1b and $p16^{Ink4a}$ exon 1a in $Bmi1^{-/-}$ MEFs. Wild-type and $Bmi1^{-/-}$ MEFs (P-2) pretreated with 10 mM NAC were subjected to ChIP analyses using the indicated antibodies. Percentages of input DNA are shown as the mean ± S.D. for multiple experiments (n>5). Statistical significance was determined with Student's t-test; $*p<0.05$, $**p<0.01$, $***p<0.001$.
doi:10.1371/journal.pone.0012373.g006

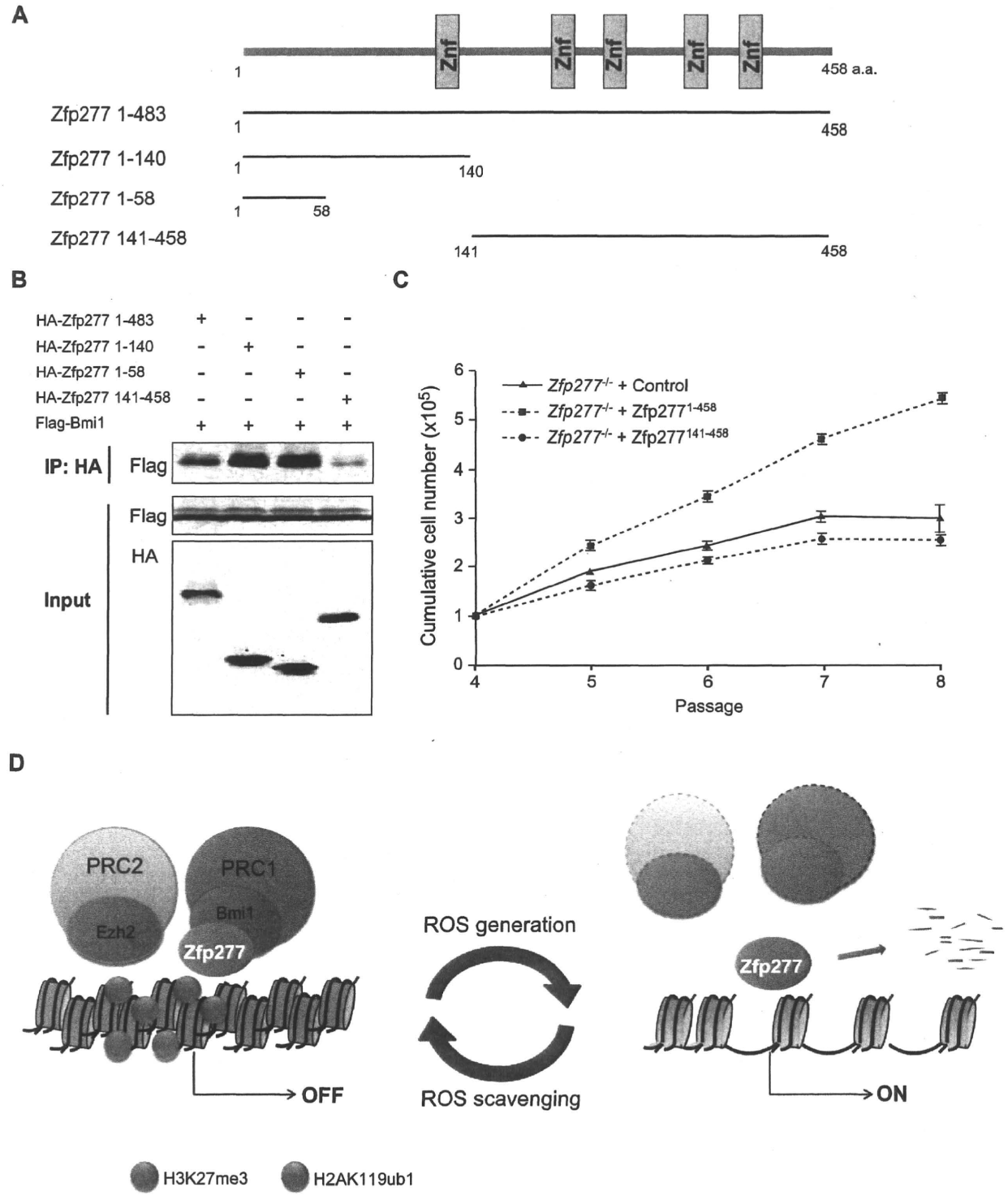

Figure 7. Zfp277 suppresses the *Ink4a/Arf* locus through interaction with Bmi1. A. A schematic representation of the deletion mutants of Zfp277. Znf represents a Zinc finger domain. **B.** HA-tagged deletion mutants of Zfp277 and Flag-tagged Bmi1 were cotransfected into 293T cells. After 48 hrs of transfection, the Zfp277 deletion mutants were immunoprecipitated using an anti-HA antibody and the immunoprecipitates were subjected to Western blotting with an anti-Flag or HA antibody. **C.** The growth curve of *Zfp277*$^{-/-}$ MEFs expressing Zfp277 deletion mutants. *Zfp277*$^{-/-}$ MEFs (P-3) were transduced with a control, *Zfp277*$^{1-458}$, or *Zfp277*$^{141-458}$ retrovirus and cell growth was monitored every three days by replating at 1×10^5 cells/plate. Cumulative cell numbers are shown as the mean ± SD for three independent triplicate experiments. **D.** A scheme for the dynamic regulation of PcG function in response to oxidative stress. The generation or scavenging of ROS leads to eviction or restoration of Zfp277 and PcG at the *Ink4a/Arf* locus. In this cycle, Zfp277 plays an essential role in the re-localization of PRC1 but not PRC2 in response to the scavenging of ROS.
doi:10.1371/journal.pone.0012373.g007

[53]. Furthermore, *Mel18*$^{-/-}$ MEFs undergo p19^{Arf}-dependent premature senescence like *Bmi1*$^{-/-}$ MEFs [54]. Our findings indicate that Mel18 behaves as a back-up molecule for Bmi1 in gene silencing of *Ink4a/Arf* in *Zfp277*$^{-/-}$ and *Bmi1*$^{-/-}$ MEFs treated with NAC, thus supporting the notion of functional redundancy between Bmi1 and Mel18. However, the specific collaboration between Zfp277 and Bmi1-containing PRC1 also highlights the difference in properties between Bmi1- and Mel18-containing PRC1.

Although Zfp277 is not responsible for the recruitment of Ezh2 and Mel18, the binding of these two proteins to the *Ink4a/Arf* locus was profoundly affected in *Zfp277*$^{-/-}$ MEFs (Figure 4). This might be attributed to enhanced oxidative stress, as evident in Figure S3, which causes a reduction in the levels of Ezh2 and Mel18 (Figure 3A). This notion is supported by the results of ChIP experiments with NAC-treated *Zfp277*$^{-/-}$ MEFs in which the recovery in binding of Ezh2 and Mel18 to the *Ink4a/Arf* locus was well correlated with the recovery of their protein levels. In the same experiments, the H3K27me3 levels were reduced to background levels, although the reduction in Ezh2 binding was not so drastic in *Zfp277*$^{-/-}$ MEFs (Figure 4). This discrepancy could be explained by the enhanced recruitment of Jmjd3, an H3K27me2/3 demethylase, to the *Ink4a/Arf* locus. Furthermore, it is hypothesized that there is an interdependence of PRC1 and PRC2 binding and function [41]. These factors could account for a significant reduction in H3K27me3 at the *Ink4a-Arf* locus in *Zfp277*$^{-/-}$ MEFs.

Expression of p16^{Ink4a} increases markedly in aging mouse and human tissues, linking *Ink4a/Arf* with the aging process [55]. Importantly, numerous studies have shown that aging is closely associated with oxidative damage. For example, the generation of ROS leads to a cell-autonomous functional decline of hematopoietic stem cells which normally exhibit low levels of ROS. Conversely, NAC treatment prevents the stress-induced loss of hematopoietic stem cells [56]. In this study, we observed that ROS profoundly affected the functions of both Zfp277 and PcG proteins and induced JNK activation, resulting in deregulation of the *Ink4a/Arf* locus. Thus, our results raise the possibility that Zfp277 is involved in the regulation of aging and stem cell function through collaborative regulation of the *Ink4a/Arf* locus with PcG complexes.

Materials and Methods

Plasmids and antibodies

Full-length mouse *Zfp277* (NM_178845) was cloned by RT-PCR using mouse hematopoietic progenitor cDNA. HA-tagged *Zfp277* and deletion mutants, Flag-tagged *Bmi1* fused with *GFP*, Flag-tagged *Ring1B*, Flag-tagged *Ezh2*, and Myc-tagged *Mel18* were subcloned into pcDNA3 (Invitrogen). Flag-tagged *Bmi1* fused with *GFP* was also subcloned into CSII-EF-1α lentivirus vector. Full-length *Zfp277* and Zfp277$^{141-458}$ were subcloned into a retroviral vector, MSCV-EF-1-EGFP. The GST fused with Zfp277 or Bmi1 was subcloned into pGEX6p-1 expression vectors (Invitrogen). The retroviral vector encoding Bmi1 was described previously [57]. pMYs-E6-ires-EGFP was kindly provided by Dr. T. Kiyono (National Cancer Center, Tokyo, Japan). A polyclonal antibody against Zfp277 was generated by immunizing rabbits with recombinant N-terminal Zfp277 (a.a. 1–170).

Generation of Zfp277 knockout mice and preparation of MEFs

Gene targeting of *Zfp277* was performed as described previously [58]. Briefly, a gene-targeting vector was generated using a BAC clone containing the *Zfp277* gene obtained from a mouse 129/Sv BAC library (Invitrogen). The targeting strategy is shown in Figure S1. The linealized targeting vector was introduced into R1 ES cells by electroporation and the cells were subjected to selection using G418. G418-resistant clones were isolated and recombination was confirmed by Southern blotting using an internal probe. Germline chimeras were generated by an aggregation method. Germline transmission of the target allele was confirmed by PCR using DNA from the tail. Mice were bred and maintained in the Animal Research Facility of the Graduate School of Medicine, Chiba University in accordance with our institutional guidelines. This study was approved by the institutional review committees of Chiba University (approval numbers 21–65 and 21–150). MEFs prepared from E12.5 embryos were cultured in Dulbecco's modified Eagle's medium (DMEM) supplemented with 10% fetal bovine serum and a 1% penicillin-streptomycin mixture (Sigma) at 37°C under 10% CO2 in a humidified incubator and passaged every three days.

Cell proliferation assay, β-galactosidase staining, and antioxidant treatment

For the cell proliferation assay, wild-type, *Zfp277*$^{-/-}$, and *Bmi1*$^{-/-}$ MEFs were seeded at 1×10^5 cells/well in 6-cm plates and cultured at 37°C in 10% CO2 in a humidified incubator. Viable cells were counted every three days by Trypan Blue exclusion, and then replated at 1×10^5 cells/well. Antioxidant treatment was performed by adding 10 mM NAC (Sigma) to the medium. For the staining of β-galactosidase, cells were fixed with 3% formaldehyde and 0.025% glutaraldehyde (Sigma) for 5 min, and incubated with citrate buffer (pH 5.2) containing FeCN for 2 to 16 hrs before images were taken.

RNA extraction, reverse transcription and quantitative PCR analysis

Total RNA was extracted from cells at 75% confluency using Trizol LS® total RNA isolation reagent (Gibco BRL, Life Technologies) according to the manufacturer's instructions. cDNA was synthesized from total RNA using the Superscript II First Strand Synthesis System (Invitrogen). Quantitative RT-PCR was performed with an ABI Prism® 7300 Sequence Detector (Applied Biosystems). Universal Library probe assays were performed using the LightCycler® FastStart universal probe master (PE Applied Biosystems), an optimal combination of universal probe, and gene-specific primer sets designed by the Universal ProbeLibrary assay design center (https://www.roche-applied-science.com) (Table S1). The reactions were conducted in a 96-well optical plate at 95°C for 10 min, followed by 40 cycles of 95°C for 5 sec and 60°C for 31 sec. The Ct data was determined with default threshold settings.

Immunoprecipitation, co-Immunoprecipitation, and Western blot analyses

For immunoprecipitation and co-immunoprecipitation analyses, cells were lysed in hypertonic lysis buffer [20 mM sodium phosphate at pH 7.0, 250 mM NaCl, 0.1% NP-40, 30 mM $Na_4P_2O_7$, 10 mM NaF, 5 mM EDTA, 1 mM DDT, and a protease inhibitor cocktail (Complete Midi, Roche)] at 4°C for more than 40 min, sonicated, and subjected to immunoprecipitation as described previously [27]. Proteins were analyzed by SDS-PAGE, transferred to a PVDF membrane (Immobilon™; Millipore), and detected by Western blotting using the following antibodies; HA (sc-805, Y-11), and p16^{Ink4a} (sc-468, C-20)(Santa Cruz); Bmi1 (05-637, F6), H3K27me3 (07-449)(Millipore); Kdm6b/Jmjd3 (ab38113), p19^{Arf} (ab80)(Ab-

cam); α-Tubulin (T6074, B-5-1-2)(Sigma); phosphor-Sapk/Jnk (Thr183/Try185)(#9251) (Cellsignal); Ezh2 (BD43) [59], and mouse anti-Ring1B monoclonal antibody [60].

Chromatin immunoprecipitation assay

ChIP assays were performed as described previously [27]. Briefly, cells were fixed with 1% formaldehyde for 15 min and then incubated in the presence of 0.125 M Glycine for 10 min. The cells were lysed with lysis buffer [(50 mM Tris-HCl (pH 8.0), 10 mM EDTA, 0.1%SDS, and a proteinase inhibitor cocktail (Complete Midi)) on ice for 20 min and sonicated. The lysate was separated into three samples diluted with an equal volume of dilution buffer [50 mM Tris-HCl (pH 8.0), 150 mM NaCl, 1%Triton X-100, 0.1%SDS, and a proteinase inhibitor cocktail (Complete Midi)]. Immunoprecipitation was performed overnight at 4°C using anti-Bmi1 (clone 8A9, kindly provided by Dr. N. Nozaki, MAB Institute, Co. Ltd., Japan), anti-monoubiquitinated H2A (H2Aub1) (E6C5, Millipore), anti-rabbit IgG, anti-mouse IgG, anti-Ring1B, anti-Kdm6b/Jmjd3, anti-Mel18 (sc-10744, H-115)(SantaCruz), anti-Ezh2 (AC22)[55], anti-HA, anti-H3K27me3, and anti-Zfp277 antibodies. For anti-H2Aub1, chromatin was immunoprecipitated overnight at 4°C with anti-H2Aub1, followed by the addition of anti-mouse IgMμ (12-488, Millipore) and further incubation for 2 hours at 4°C. After the immunoprecipitation, 25 ml of salmon sperm DNA/Protein G and A sepharose beads was added and incubated for 1 hr at 4°C. The immunoprecipitates were washed extensively and subjected to a Q-PCR analysis by SYBR Premix Ex Taq™ II (Takara) using the primers listed in Supplemental Table S1 [33].

Supporting Information

Figure S1
Found at: doi:10.1371/journal.pone.0012373.s001 (2.29 MB EPS)

Figure S2
Found at: doi:10.1371/journal.pone.0012373.s002 (1.74 MB EPS)

Figure S3
Found at: doi:10.1371/journal.pone.0012373.s003 (1.65 MB EPS)

Figure S4
Found at: doi:10.1371/journal.pone.0012373.s004 (1.38 MB EPS)

Table S1
Found at: doi:10.1371/journal.pone.0012373.s005 (1.50 MB EPS)

Acknowledgments

We thank Naohito Nozaki for the anti-Bmi1 antibody and members of the Iwama laboratory for technical advice and helpful discussions.

Author Contributions

Conceived and designed the experiments: MN AI. Performed the experiments: MN AS SM. Analyzed the data: MN KH HK AI. Contributed reagents/materials/analysis tools: KH HK. Wrote the paper: MN AI.

References

1. Kim WY, Sharpless NE (2006) The Regulation of INK4/ARF in Cancer and Aging. Cell 127: 265–275.
2. Collado M, Blasco MA, Serrano M (2007) Cellular Senescence in cancer and aging. Cell 130: 223–233.
3. Sherr CJ (2001) The INK4a/ARF network in tumour suppression. Nat Rev Mol Cell Biol 2: 731–737.
4. Adams PD (2009) Healing and hurting: molecular mechanisms, functions, and pathologies of cellular senescence. Mol Cell 36: 2–14.
5. Gil J, Peters G (2006) Regulation of the INK4b-ARF-INK4a tumour suppressor locus: all for one or one for all. Nat Rev Mol Cell Biol 7: 667–677.
6. Carnero A, Hudson JD, Price CM, Beach DH (2000) p16INK4A and p19ARF act in overlapping pathways in cellular immortalization. Nat Cell Biol 2: 148–155.
7. Krimpenfort P, Quon KC, Mooi WJ, Loonstra A, Berns A (2001) Loss of p16Ink4a confers susceptibility to metastatic melanoma in mice. Nature 413: 83–86.
8. Sharpless NE, Bardeesy N, Lee KH, Carrasco D, Castrillon DH, et al. (2001) Loss of $p16^{Ink4a}$ with retention of $p19^{Arf}$ predisposes mice to tumorigenesis. Nature 413: 86–91.
9. Rangarajan A, Weinberg RA (2003) Comparative biology of mouse versus human cells: modeling human cancer in mice. Nat Rev Cancer 3: 952–959.
10. Campisi J, d'Adda di Fagagna F (2007) Cellular senescence: when bad things happen to good cells. Nat Rev Mol Cell Biol 8: 729–740.
11. Simon JA, Kingston RE (2009) Chromatin dynamics Mechanisms of Polycomb gene silencing: knowns and unknowns. Nat Rev Mol Cell Biol 10: 697–708.
12. Pietersen AM, and van Lohuizen M (2008) Stem cell regulation by polycomb repressors: postponing commitment. Curr Opin Cell Biol 20: 201–207.
13. Park IK, Qian D, Kiel M, Becker MW, Pihalja M, et al. (2003) Bmi-1 is required for maintenance of adult self-renewing haematopoietic stem cells. Nature 423: 302–305.
14. Molofsky AV, Pardal R, Iwashita T, Park IK, Clarke MF, et al. (2003) Bmi-1 dependence distinguishes neural stem cell self-renewal from progenitor proliferation. Nature 425: 962–967.
15. Jacobs JJ, Kieboom K, Marino S, DePinho RA, van Lohuizen M (1999) The oncogene and Polycomb-group gene bmi-1 regulates cell proliferation and senescence through the ink4a locus. Nature 397: 164–168.
16. Itahana K, Zou Y, Itahana Y, Martinez JL, Beausejour C, et al. (2003) Control of the replicative life span of human fibroblasts by p16 and the polycomb protein Bmi-1. Mol Cell Biol 23: 389–401.
17. Gil J, Bernard D, Martínez D, Beach D (2004) Polycomb CBX7 has a unifying role in cellular lifespan. Nat Cell Biol 6: 67–72.
18. Iwama A, Oguro H, Negishi M, Kato Y, Morita Y, et al. (2004) Enhanced self-renewal of hematopoietic stem cells mediated by the polycomb gene product Bmi-1. Immunity 21: 843–851.
19. Oguro H, Iwama A, Morita Y, Kamijo T, van Lohuizen M, et al. (2006) Differential impact of Ink4a and Arf on hematopoietic stem cells and their bone marrow microenvironment in Bmi1-deficient mice. J Exp Med 203: 2247–2253.
20. Bracken AP, Helin K (2009) Polycomb group proteins: navigators of lineage pathways led astray in cancer. Nat Rev Cancer 9: 773–782.
21. Schuettengruber B, Cavalli G (2009) Recruitment of polycomb group complexes and their role in the dynamic regulation of cell fate choice. Development 136: 3531–3542.
22. Wang L, Brown JL, Cao R, Zhang Y, Kassis JS (2004) Hierarchical recruitment of polycomb group silencing complexes. Mol Cell 14: 637–646.
23. Wang H, Wang L, Erdjument-Bromage H, Vidal M, Tempst P, et al. (2004) Role of histone H2A ubiquitination in Polycomb silencing. Nature 431: 873–878.
24. de Napoles M, Mermoud JE, Wakao R, Tang YA, Endoh M, et al. (2004) Polycomb group proteins Ring1A/B link ubiquitylation of histone H2A to heritable gene silencing and X inactivation. Dev Cell 7: 663–676.
25. Cao R, Tsukada Y, Zhang Y (2005) Role of Bmi-1 and Ring1A in H2A ubiquitylation and Hox gene silencing. Mol Cell 20: 845–854.
26. Stock JK, Giadrossi S, Casanova M, Brookes E, Vidal M, et al. (2007) Ring1-mediated ubiquitination of H2A restrains poised RNA polymerase II at bivalent genes in mouse Es cells. Nat Cell Biol 9: 1428–135.
27. Negishi M, Saraya A, Miyagi S, Nagao K, Inagaki Y, et al. (2007) Bmi1 cooperates with Dnmt1-associated protein 1 in gene silencing. Biochem Biophys Res Commun 353: 992–998.
28. Liang H, Guo W, Nagarajan L (2000) Chromosomal mapping and genomic organization of an evolutionarily conserved zinc finger gene ZNF277. Genomics 66: 226–228.
29. Lennon PA, Cooper ML, Peiffer DA, Gunderson KL, Patel A, et al. (2007) Deletion of 7q31.1 supports involvement of FOXP2 in language impairment. Am J Med Genet 143: 791–798.
30. Bracken AP, Kleine-Kohlbrecher D, Dietrich N, Pasini D, Gargiulo G, et al. (2007) The polycomb group proteins bind throughout the INK4A-ARF locus and are dissociated in senescent cells. Genes & Dev 21: 525–530.
31. Agger K, Cloos PA, Rudkjaer L, Williams K, Andersen G, et al. (2009) The H3K27me3 demethylase JMJD3 contributes to the activation of the INK4A-ARF locus in response to oncogene- and stress-induced senescence. Genes & Dev 23: 1171–1176.
32. Barradas M, Anderton E, Acosta JC, Li S, Banito A, et al. (2009) Histone demethylase JMJD3 contributes to epigenetic control of INK4a/ARF by oncogenic RAS. Genes & Dev 23: 1177–1182.
33. Tzatsos A, Pfau R, Kampranis SC, Tsichlis PN (2009) Ndy1/KDM2B immortalizes mouse embryonic fibroblasts by repressing the Ink4a/Arf locus. Proc Natl Acad Sci U S A 106: 2641–2646.

34. Parrinello S, Samper E, Krtolica A, Goldstein J, Melov S, et al. (2003) Oxygen sensitivity severely limits the replicative lifespan of murine fibroblasts. Nat Cell Biol 5: 741–747.
35. Chen Q, Ames BN (1994) Senescence-like growth arrest induced by hydrogen peroxide in human diploid fibroblast F65 cells. Proc Natl Acad Sci USA 91: 4130–4134.
36. Macip S, Igarashi M, Fang L, Chen A, Pan ZQ, et al. (2002) Inhibition of p21-mediated ROS accumulation can rescue p21-induced senescence. EMBO J 21: 2180–2188.
37. Elderkin S, Maertens GN, Endoh M, Mallery DL, Morrice N, et al. (2007) A phosphorylated form of Mel-18 targets the Ring1B histone H2A ubiquitin ligase to chromatin. Mol Cell 28: 107–120.
38. Kranc KR, Bamforth SD, Bragança J, Norbury C, van Lohuizen M, et al. (2003) Transcriptional coactivator cited2 induces Bmi1 and Mel18 and controls fibroblast proliferation via Ink4a/ARF. Mol Cell Biol 23: 7658–7666.
39. Liu J, Cao L, Chen J, Song S, Lee IH, et al. (2009) Bmi1 regulates mitochondrial function and the DNA damage response pathway. Nature 459: 387–392.
40. Muller J, Kassis JA (2006) Polycomb response elements and targeting of polycomb group proteins in *Drosophila*. Curr Opin Genet Dev 16: 476–484.
41. Sing A, Pannell D, Karaiskakis A, Sturgeon K, Djabali M, et al. (2009) A vertebrate polycomb response element governs segmentation of the posterior hindbrain. Cell 138: 885–897.
42. Woo CJ, Kharchenko PV, Daheron L, Park PJ, Kingston RE (2010) A region of the human HOXD cluster that confers polycomb-group responsiveness. Cell 140: 99–110.
43. Herz H-M, Shilatifard A (2010) The JARID2-PRC2 duality. Genes & Den 24: 857–861.
44. Dietrich N, Bracken AP, Trinh E, Schjerling CK, Koseki H, et al. (2007) Bypass of senescence by the polycomb group protein CBX8 through direct binding to the INK4A-ARF locus. EMBO J 26: 1637–1648.
45. Maertens GN, El Messaoudi-Aubert S, Racek T, Stock JK, Nicholls J, et al. (2009) Several distinct polycomb complexes regulate and co-localize on the INK4a tumor suppressor locus. PLoS One 28: e6380.
46. Bernstein E, Duncan EM, Masui O, Gil J, Heard E, et al. (2006) Mouse polycomb proteins bind differentially to methylated histone H3 and RNA and are enriched in facultative heterochromatin. Mol Cell Biol 26: 2560–2569.
47. Ren X, Vincenz C, Kerppola TK (2008) Changes in the distributions and dynamics of polycomb repressive complexes during embryonic stem cell differentiation. Mol Cell Biol 28: 2884–2895.
48. Schoeftner S, Sengupta AK, Kubicek S, Mechtler K, Spahn L, et al. (2006) Recruitment of PRC1 function at the initiation of X inactivation independent of PRC2 and silencing. EMBO J 25: 3110–3122.
49. Barna M, Merghoub T, Costoya JA, Ruggero D, Branford M, et al. (2002) Plzf mediates transcriptional repression of HoxD gene expression through chromatin remodeling. Dev Cell 3: 499–510.
50. Lee N, Maurange C, Ringrose L, Paro R (2009) Suppression of Polycomb group proteins by JNK signalling induces transdetermination in Drosophila imaging discs. Nature 438: 234–237.
51. Owusu-Ansah E, Banerjee U (2009) Reactive oxygen species prime Drosophila haematopoietic progenitors for differentiation. Nature 461: 537–541.
52. van der Lugt NM, Domen J, Linders K, van Roon M, Robanus-Maandag E, et al. (1994) Posterior transformation, neurological abnormalities, and severe hematopoietic defects in mice with a targeted deletion of the bmi-1 proto-oncogene. Genes & Dev 8: 757–769.
53. Akasaka T, van Lohuizen M, van der Lugt N, Mizutani-Koseki Y, Kanno M, et al. (2001) Mice doubly deficient for the Polycomb Group genes Mel18 and Bmi1 reveal synergy and requirement for maintenance but not initiation of Hox gene expression. Development 128: 1587–1597.
54. Miki J, Fujimura Y, Koseki H, Kamijo T (2007) Polycomb complexes regulate cellular senescence by repression of ARF in cooperation with E2F3. Genes Cells 12: 1371–1382.
55. Krishnamurthy J, Torrice C, Ramsey MR, Kovalev GI, Al-Regaiey K, et al. (2004) Ink4a/Arf expression is a biomarker of aging. J Clin Invest 114: 1299–1307.
56. Ito K, Hirao A, Arai F, Takubo K, Matsuoka S, et al. (2006) Reactive oxygen species act through p38 MAPK to limit the lifespan of hematopoietic stem cells. Nat Med 12: 446–451.
57. Chiba T, Zheng YW, Kita K, Yokosuka O, Saisho H, et al. (2007) Enhanced self-renewal capability in hepatic stem/progenitor cells drives cancer initiation. Gastroenterology 133: 937–950.
58. Fukamachi H, Fukuda K, Suzuki M, Furumoto T, Ichinose M, et al. (2001) Mesenchymal transcription factor Fkh6 is essential for the development and differentiation of parietal cells. Biochem Biophys Res Commun 280: 1069–1076.
59. Pasini D, Bracken AP, Jensen MR, Lazzerini Denchi E, et al. (2004) Suz12 is essential for mouse development and for EZH2 histone methyltransferase activity. EMBO J 23: 4061–4071.
60. Atsuta T, Fujimura S, Moriya H, Vidal M, Akasaka T, et al. (2001) Production of monoclonal antibodies against mammalian Ring1B proteins. Hybridoma 20: 43–46.

Oncogene (2011) 30, 97–105

www.nature.com/onc

ORIGINAL ARTICLE

CD133 suppresses neuroblastoma cell differentiation via signal pathway modification

H Takenobu[1], O Shimozato[2], T Nakamura[3], H Ochiai[1,4], Y Yamaguchi[1], M Ohira[5], A Nakagawara[6] and T Kamijo[1]

[1]Division of Biochemistry and Molecular Carcinogenesis, Chiba Cancer Center Research Institute, Chiba, Japan; [2]Laboratory of Anti-tumor Research, Chiba Cancer Center Research Institute, Chiba, Japan; [3]Core Facility for Therapeutic Vectors, The Institute of Medical Science, The University of Tokyo, Tokyo, Japan; [4]Department of Pediatrics, Graduate School of Medicine, Chiba University, Chiba, Japan; [5]Laboratory of Cancer Genomics, Chiba Cancer Center Research Institute, Chiba, Japan and [6]Division of Biochemistry and Innovative Cancer Therapeutics, Chiba Cancer Center Research Institute, Chiba, Japan

CD133 (prominin-1) is a transmembrane glycoprotein expressed on the surface of normal and cancer stem cells (tumor-initiating cells), progenitor cells, rod photoreceptor cells and a variety of epithelial cells. Although CD133 is widely used as a marker of various somatic and putative cancer stem cells, its contribution to the fundamental properties of cancer cells, such as tumorigenesis and differentiation, remains to be elucidated. In the present report, we found that CD133 was expressed in several neuroblastoma (NB) cell lines/tumor samples. Intriguingly, CD133 repressed NB cell differentiation, for example neurite extension and the expression of differentiation marker proteins, and was decreased by several differentiation stimuli, but accelerated cell proliferation, anchorage-independent colony formation and *in vivo* tumor formation of NB cells. NB cell line and primary tumor-sphere experiments indicated that the molecular mechanism of CD133-related differentiation suppression in NB was in part dependent on neurotrophic receptor RET tyrosine kinase regulation. RET transcription was suppressed by CD133 in NB cells and glial cell line-derived neurotrophic factor treatment failed to induce RET in CD133-expressing cells; RET overexpression rescued CD133-related inhibition of neurite elongation. Of note, CD133-related NB cell differentiation and RET repression were mainly dependent on p38MAPK and PI3K/Akt pathways. Furthermore, CD133 has a function in growth and RET expression in NB cell line- and primary tumor cell-derived tumor spheres. To the best of our knowledge, this is the first report of the function of CD133 in cancer cells and our findings may be applied to improve differentiation induction therapy for NB patients.
Oncogene (2011) **30**, 97–105; doi:10.1038/onc.2010.383; published online 6 September 2010

Keywords: CD133; neuroblastoma; differentiation; RET p38MAPK; PI3K/Akt

Correspondence: Professor T Kamijo, Division of Biochemistry and Molecular Carcinogenesis, Chiba Cancer Center Research Institute, 666-2 Nitona, Chuo-ku, Chiba 260-8717, Japan.
E-mail: tkamijo@chiba-cc.jp
Received 2 March 2010; revised 5 July 2010; accepted 14 July 2010; published online 6 September 2010

Introduction

CD133 (AC133; human prominin-1) belongs to a family of cell-surface glycoproteins harboring five transmembrane domains (Corbeil *et al.*, 2001) and was originally found as a hematopoietic stem cell marker (Yin *et al.*, 1997). CD133 was subsequently shown to be expressed by a number of progenitor cells, including those of the epithelium, where it is expressed on the apical surface (Corbeil *et al.*, 2000). Previously, it was found that CD133-expressing cells in brain tumors have the capacity for unlimited self-renewal, as well as the ability, in small numbers, to initiate tumor formation and progression in immuno-deficient mice (Singh *et al.*, 2004), suggesting that CD133-expressing cells satisfy the important criteria required for tumor-initiating cells (TICs) (Reya *et al.*, 2001; Jordan *et al.*, 2006). Using similar methods, CD133 has recently been designated as a marker associated with TICs in the colon (O'Brien *et al.*, 2007; Ricci-Vitiani *et al.*, 2007), pancreatic (Olempska *et al.*, 2007), liver (Yin *et al.*, 2007), skin (Monzani *et al.*, 2007) and prostate (Collins *et al.*, 2005; Miki *et al.*, 2007) cancers. Maw *et al.* (2000) reported homozygosity for a 1-bp deletion (1878delG) in exon 16 of the CD133 gene predicted to cause a frameshift at codon 614 and a prematurely truncated protein lacking about half of the second extracellular loop, the final membrane-spanning segment and the cytoplasmic-C-terminal domain; this missense mutation caused retinal degeneration in four affected members of a consanguineous Indian family. This finding was further confirmed by an article describing that loss of Prom-1 in genetically modified mouse results in the progressive degeneration of mature photoreceptors with complete loss of vision (Zacchigna *et al.*, 2009); however, to the best of our knowledge, no reports have studied the function of CD133 in tumorigenesis.

Neuroblastoma (NB) is the most common pediatric solid malignant tumor derived from the sympathetic nervous system. Unlike the many childhood malignancies for which survival has been improved by recent therapies, high-risk NB is still one of the most difficult tumors to cure, with only 30% long-term survival despite intensive multimodal therapy (Maris *et al.*,

2007). The clinical presentation and treatment response of advanced NB, which results in relapse and a refractory state after a good responsive to the initial chemotherapy, suggest that TICs likely exist in NB tumors. A previous report indicated the isolation and characterization of putative TICs using primary-sphere formation with tumors and bone marrow metastases from NB patients, although CD133 expression was not detected in a bone marrow-derived high-risk NB tumorsphere sample (Hansford *et al.*, 2007). On the other hand, it was reported that sub-cloned NB cells (designated 'intermediate type'), which have a significantly more malignant phenotype, with four- to fivefold greater plating efficiencies in soft agar and sixfold higher tumorigenicity in athymic mice, expressed high amounts of CD133 mRNA compared with less malignant subclones (Walton *et al.*, 2004); therefore, the function of CD133 in NB tumorigenesis and aggressiveness remains unresolved.

Previous reports about CD133 expression in NB and its function as a stem cell marker in several tumors prompted us to study the function of CD133 in NB cells (Walton *et al.*, 2004; Hansford *et al.*, 2007). Our results clearly indicated that CD133 also seems to regulate cell proliferation and tumorigenesis in NB cells. Importantly, CD133 represses NB cell differentiation and is decreased by several differentiation stimulators. We studied the molecular mechanism of CD133-related differentiation inhibition in NB cells and found that it was in part dependent on RET tyrosine kinase receptor regulation via signal pathway modification. Furthermore, CD133 is expressed in NB cell spheres and has a function in sphere growth and RET regulation.

In specific malignancies, for example NB and acute promyelocytic leukemia, differentiation induction therapy using retinoic acid is clearly effective. *In vitro* experiments indicated that all-*trans*-retinoic acid (ATRA) treatment induced morphological and biochemical differentiation in these cancer cells, suggesting that the induced differentiation seems to repress the tumorigenic activity of cancer cells (Brodeur *et al.*, 2000; Weinberg, 2006). Together, CD133 may regulate NB tumorigenesis and proliferation by preventing differentiation.

Results

CD133 has a function in NB cell proliferation

First, we checked the expression of CD133 in NB cell lines and found its expression in 7 out of 20 (53%) cell lines (Figure 3d and Supplementary Figure 1S). A high level of cell-surface expression of *CD133* was detected in TGW and SK-N-DZ cells, and modest expression was found in IMR32 (Figure 1a; Supplementary Figure 1Sa). Next, we knocked down *CD133* in highly expressing NB cells and analyzed the knockdown-induced phenotype. Figure 1b shows that infection of shRNA-reduced CD133 mRNA and protein and *CD133* knockdown in TGW cells effectively resulted in significant growth retardation. Inhibition of cell proliferation by CD133 small-interference RNA was also observed in SK-N-DZ cells (Supplementary Figure S1). Furthermore, stable knockdown of *CD133* in TGW cells suppressed cell proliferation under anchorage-independent conditions (Figure 1c). To test tumorigenicity *in vivo*, *CD133*-silenced TGW cells were injected subcutaneously into nude mice. Mock shRNA lentivirus-infected cells formed large tumors within 9 days post-injection; CD133 shRNA lentivirus-infected cells formed very small tumors (Figure 1d). Next, we examined the effect of CD133 on NB cell proliferation (Supplementary Figure 2S). CD133 was successfully expressed in SH-SY5Y cells by lentivirus. The proliferation rate of CD133-expressing SH-SY5Y cells was 2–2.5-fold greater than mock cells. Moreover, a soft agar colony formation assay showed that CD133-expressing cells formed more and bigger colonies than mock-control cells.

CD133 knockdown induces NB differentiation

In NB cells, differentiation into a neuronal phenotype is induced when cells are treated with several stimulations. Glial cell line-derived neurotrophic factor (GDNF) induced neurite outgrowth in TGW cells (Figure 2a, center). In CD133 knocked-down TGW cells, neurite formation was observed even under normal culture conditions (Figure 2a, KD). We scored cells with neurite length longer than the cell body diameter as neurite positive (Figure 2b). CD133 knocked-down cells showed intensified neurite extensions when compared with mock cells. Mock-infected and CD133 knocked-down cells were collected at the end of the experiment, and mRNA was extracted and subjected to RT–PCR (Figure 2c). With *GAP43/neurofilament (NF) 68* as neuronal differentiation markers, these expressions were constitutively upregulated in CD133 knocked-down cells. Along with differentiation induced by treatment with ATRA or phorbol-12-myristate-13-acetate (TPA) in parental TGW cells, CD133 expression was suppressed at both protein and mRNA levels (Supplementary Figure 3S). These results indicated that CD133 may suppress the differentiation of NB cells.

CD133 regulates RET expression in NB cells

To identify the mechanism of CD133-related cellular differentiation, we studied the expression of several neurotrophic receptors and RET receptors because they are the important signal transduction pathway molecules, which have important functions in sympathetic nerve and NB cell differentiation (Kaplan *et al.*, 1993; Klein, 1994; D'Alessio *et al.*, 1995; Enomoto *et al.*, 2001). We introduced *CD133* cDNA into several NB cell lines (Figure 3a), and checked the effect of CD133 overexpression on *RET* expression using a primer pair recognizing all *RET* isoforms, *RET51*, *RET9* and *RET43*, formed by alternative splicing of C-terminal exon cassettes (Myers *et al.*, 1995; Enomoto *et al.*, 2000). Intriguingly, in *RET* and all *RET* isoforms, transcriptions were suppressed in CD133-overexpressing NB cells (*RET* reduction was 1.3–3.8-fold by qPCR); however,

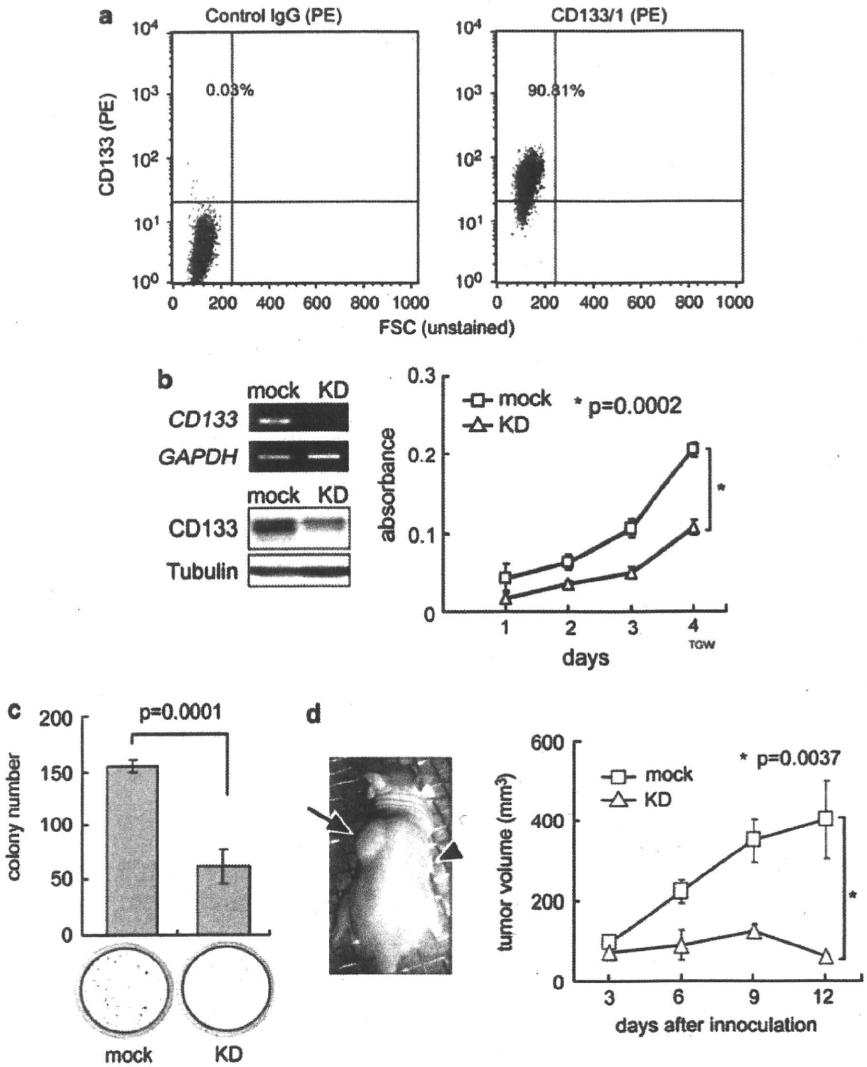

Figure 1 *CD133* knockdown inhibits the growth of human neuroblastoma (NB) cells. (**a**) Flow cytometric analysis of CD133 expression profiles in TGW cells. CD133 fluorescence is depicted on the *y* axis, and the percentage of CD133-positive cells is shown in the left upper corner of each plot. (**b**) Stable knockdown of *CD133* by lentivirus-mediated shRNA was performed as described in Materials and methods. *CD133* expression was detected by semi-quantitative RT–PCR and western blotting analysis in TGW cells. Growth curves were obtained by WST-8 assay. Anchorage-independent colony formation (**c**) and *in vivo* tumorigenic assay (**d**). TGW cells were stably transduced with shRNA against mock or CD133 (KD). (**c**) Colonies were stained with MTT dye and directly counted under a phase contrast microscope. (**d**) Tumor development in BALB/c AJcl *nu/nu* mice on injection of TGW cells stably infected with shRNA against mock (arrow) and CD133 (KD, arrowhead) cells. Tumor volume was measured every 3 days. Data are presented as the mean ± s.d. of tumors in four mice.

the effects of CD133 on *TrkA/B/C, p75NGFR* and *GDNF* expressions did not show a specific tendency. CD133 knockdown clearly increased *RET* mRNA (*RET* induction was 2.5–3.0-fold by qPCR). CD133-mediated RET downregulation was also observed at the protein level (Figure 3b). Furthermore, CD133 expression in primary NB spheres resulted in transcriptional suppression of *RET* (Figure 3c). These results suggest that CD133 suppresses *RET* gene transcription in NB cells.

To study the expression pattern of *CD133* and *RET* mRNA in human NBs, we performed semi-quantitative RT–PCR. *CD133* was expressed in 7 of 20 NB cell lines tested (Figure 3d), and only 1 NB cell line was *RET* positive in the 7 cell lines. We further studied *CD133* and *RET* expression in unfavorable patient-derived tumors (stages 3 and 4, TrkA(−), *MYCN* amplified). Again, *RET* expression was profoundly repressed in CD133-expressing NB tumors (Figure 3e). Finally, we studied the transcriptional activity of *RET* promoter in CD133-expressing cells. *RET* promoter reporter-derived luciferase activity was significantly suppressed in CD133-expressing cells (Figure 3e).

CD133 regulates NB cell differentiation in a RET-dependent manner

We investigated the biological effects of CD133 overexpression on *RET* downregulation in SH-SY5Y cells.

Significant neurite outgrowth was observed when mock-infected cells were stimulated with GDNF (Figure 4a). At the same time, no obvious difference was observed between mock- and GDNF-treated CD133-expressing cells. These results implied that CD133 overexpression inhibited NB cell differentiation.

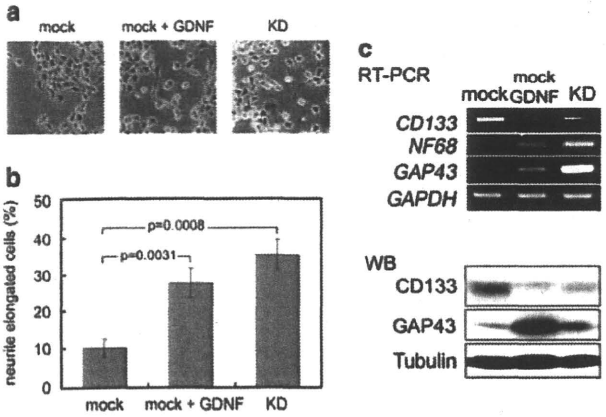

Figure 2 CD133 silencing induces differentiation in TGW cells. TGW cells were infected with lentivirus vectors encoding shRNA against *CD133* (right) or a mock (left) as a negative control. Ten days after infection, cells were treated with buffer (mock and KD) or GDNF (10 ng/ml, middle). Cells were scored for the presence of neurites longer than one cell diameter 72 h after treatment (photo: (**a**), bar graphs: (**b**)). Data are presented as the mean ± s.d. from at least three independent experiments. Statistical analysis was performed by Student's *t*-test. (**c**) NB differentiation-related molecule *neurofilament 68 (NF68)* and *GAP43* expressions in RT–PCR and WB. NF68 protein was not detected by WB in TGW cells.

We examined the effect of the co-expression of CD133 and RET (RET9) on SH-SY5Y cells. RET-expressing lentivirus was co-infected into stably CD133-expressing SH-SY5Y cells. Ten days after infection, ectopic RET and CD133 expressions were observed both at protein

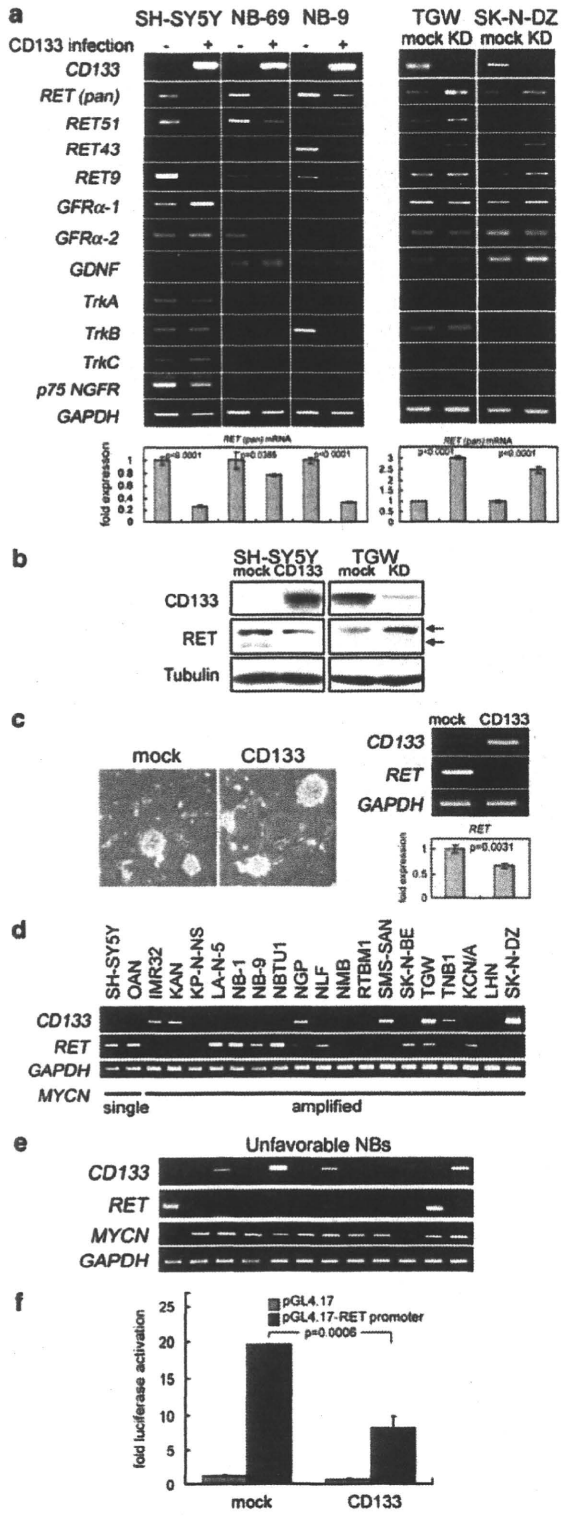

Figure 3 CD133 inhibits RET expression in NB cells. (**a**) SH-SY5Y, NB-69 and NB-9 cells were infected with mock or CD133-expressing lentivirus, and TGW and SK-N-DZ cells were stably infected with shRNA against mock or CD133 (KD) lentivirus. Semi-quantitative RT–PCR analyses were performed with CD133-modified NBs using specific primers against each *RET* isoform, *Trk* families, *GFRα-1/2* and *GDNF*. *GAPDH* was used as a loading control. Expression level of *RET* (pan) was analyzed by qPCR. In qPCR, relative *RET* values were normalized by *GAPDH*. Data are representative results of at least three independent experiments. (**b**) CD133-expressing SH-SY5Y or CD133 knocked-down TGW cell lysates were subjected to western blotting for CD133 and pan-RET expression. Pan-RET antibody detected two bands corresponding to RET isoforms (arrows). (**c**) Primary sphere from a stage 4 NB patient was infected with mock or CD133-expressing lentivirus. Five days after infection, RNA was extracted for semi-quantitative RT–PCR of *CD133*/*RET* and qPCR of *RET*. GAPDH was used as an internal control. Data are representative of three tumor samples. (**d**) Expression of *CD133* and *RET* mRNA in NB cell lines. In all, 18 NB cell lines with amplified *MYCN* and 2 cell lines with a single copy of *MYCN* were used for semi-quantitative RT–PCR analysis. (**e**) Semi-quantitative RT–PCR analysis in unfavorable primary NBs. The results of 12 NBs are shown. Unfavorable NBs: International NB Staging System (INSS) stage 3 or 4, *TrkA* (−), with *MYCN* amplified. (**f**) Effects of CD133 on *RET* promoter (0.8 kb) activity in SH-SY5Y cells. pGL4.17-*RET* promoter-driven luciferase activities were normalized to pRL-SV40 early enhancer/promoter-driven *Renilla* luciferase activities as the transfection control and expressed as relative values.

and mRNA levels (Figure 4b and data not shown). As seen in Figure 4a, GDNF significantly induced neurite outgrowth of CD133/RET co-expressing SH-SY5Y cells. CD133 single-infected cells did not respond to GDNF, suggesting that the response was dependent on RET receptor expression. However, the expression of neuronal cell differentiation markers induced by GDNF was not recovered by *RET* in CD133-expressing cells (Figure 4b). These findings indicated that CD133 inhibits GDNF-promoted neuronal differentiation via not only by *RET* but also by the other signal pathways.

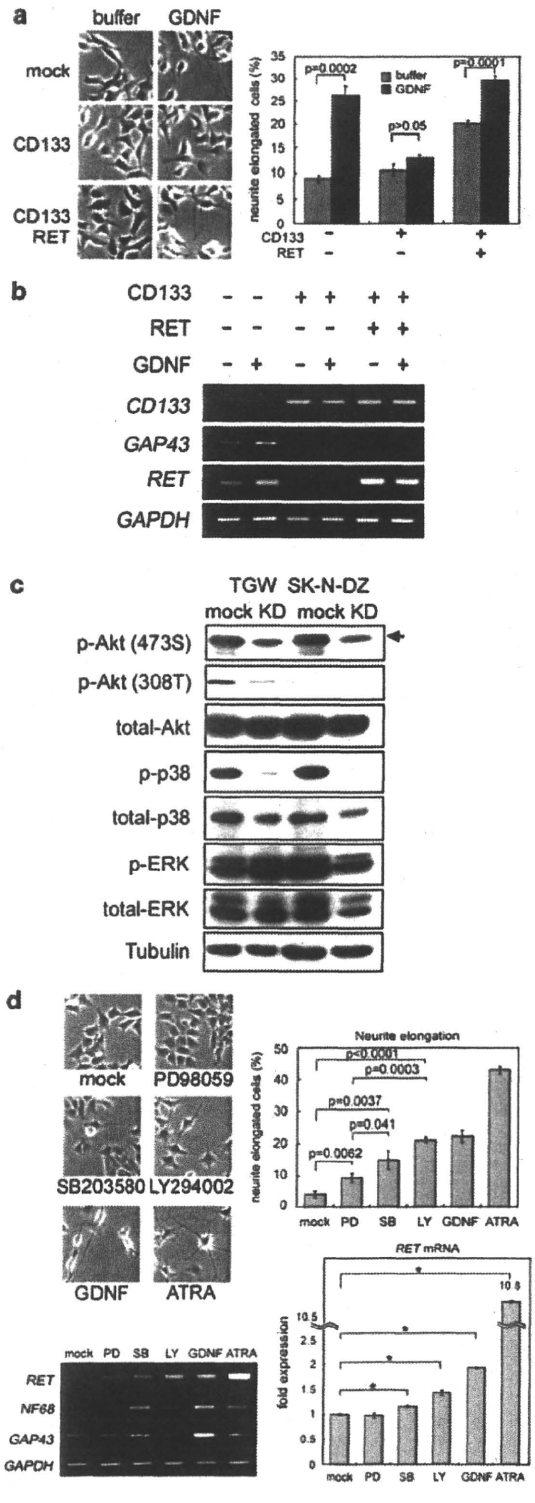

Figure 4 NB cell differentiation was regulated by CD133-dependent RET suppression via signal pathway modification. (**a**) Mock, CD133 and/or RET9 co-expressing SH-SY5Y cells were treated with GDNF (50 ng/ml) for 72 h. Cells were scored for the presence of neurites longer than one cell diameter after GDNF treatment. (**b**) CD133 and/or RET9 co-infected SH-SY5Y cells were cultured with or without GDNF treatment. Semi-quantitative RT–PCR analyses of *CD133*, *GAP43*, *RET* and *GAPDH* were performed. (**c**) The levels of phospho-Akt (p-Akt(473S) and p-Akt(308 T)), total-Akt, phospho-p38MAPK (p-p38), total-p38MAPK, phospho-ERK (p-ERK), total-ERK and tubulin were analyzed by western blot analysis. (**d**) TGW cells were cultured with DMSO (mock, 0.1%), PD98059 (PD, 5 μM), SB203580 (SB, 5 μM), LY294002 (LY, 5 μM), GDNF (50 ng/ml) or ATRA (5 μM) for 96 h. Cells were scored for the presence of neurite longer than one cell diameter after treatments. Semi-quantitative RT–PCR analysis of *RET*/*NF68*/*GAP43*/*GAPDH*, and qPCR of *RET* were performed.

CD133 regulates RET expression and NB cell differentiation by modification of signaling pathways

To identify the mechanism of *RET* downregulation in CD133-expressing cells, we studied the signaling molecule status in CD133 knocked-down cells (Figure 4c) and found a strong suppression of Akt (473S, 308T) and p38MAPK phosphorylation, but not ERK1/2 in both TGW and SK-N-DZ cells. To confirm the Akt and p38MAPK phosphorylation status caused by CD133 downregulation, we treated TGW cells with kinase inhibitors. MEK1 inhibitor (PD98059, PD), p38MAPK inhibitor (SB203580, SB) and PI3K inhibitor (LY294002, LY) induced neurite elongation in NB cells, and SB and LY were more effective for neurite elongation than PD. *RET* induction by kinase inhibitors was correlated with neurite elongation; however, differentiation markers *NF68* and *GAP43* were significantly induced by SB treatment. These results suggest that downregulation of p38MAPK and PI3K/Akt pathways has a function in CD133-related neurite elongation and differentiation marker expression is affected mainly by the p38MAPK pathway.

CD133 has a function in tumor-sphere growth and cell survival

It was previously reported that NB TICs were accumulated in NB spheres in serum-free media (SFM) (Hansford *et al.*, 2007). These observations prompted us to study the function of CD133 in tumor-sphere formation of NB cells. In IMR32 cells, only a small fraction of cells expressed CD133 (Supplementary Figure 1Sa). IMR32 cells were cultured in SFM with epidermal growth factor and fibroblast growth factor for a week, and sphere formation, upregulation of *CD133* (11.8-fold induction) and suppression of *RET* (2.8-fold reduction) were observed (Figure 5a). In primary NB cells from bone marrow metastasis,

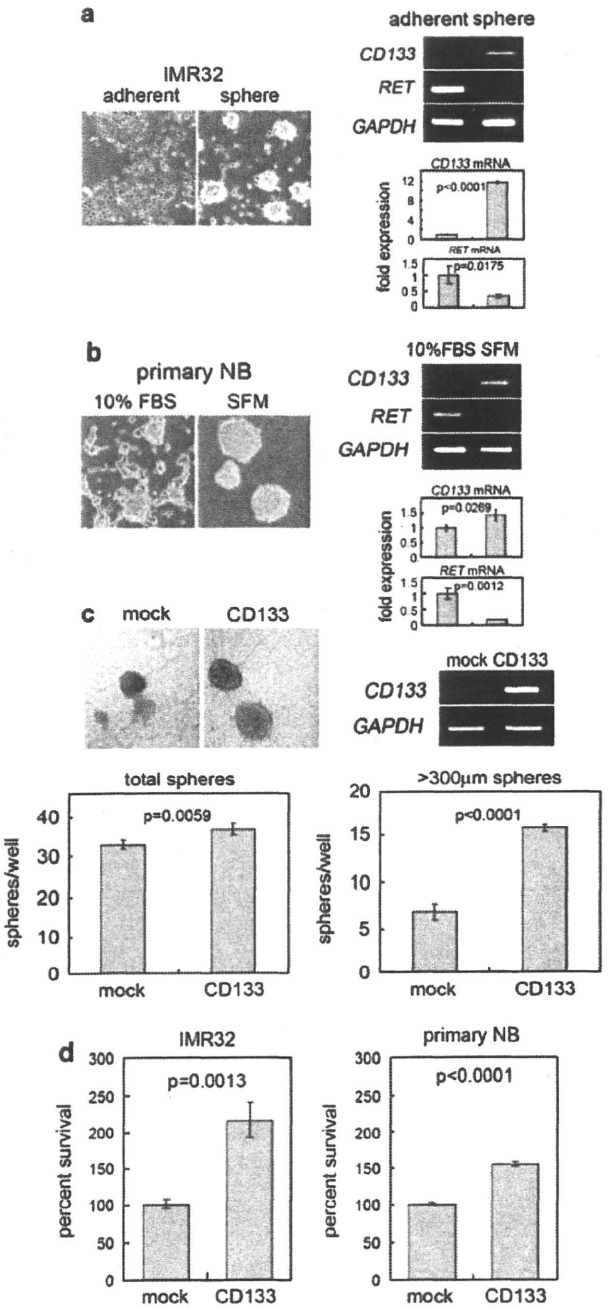

Figure 5 CD133 enhances cellular survival of NB cells in neurospheres. IMR32 cells (**a**) and primary NB cells (**b**) were cultured in 10% fetal bovine serum containing medium (adherent) or SFM (sphere) for a week. Semi-quantitative RT–PCR and qPCR analyses were performed with adherent or sphere cell RNAs using specific primers for *CD133* and *RET*. *GAPDH* was used as a loading control. Primary NB cell results are representative of three tumor samples. (**c**) IMR32 cells were stably infected with mock or CD133-expressing lentivirus. The expression levels of *CD133* and *GAPDH* were determined by semi-quantitative RT–PCR. Cells were cultured in 96-well culture plates with SFM. After 5 weeks, spheres were measured and counted under a microscope with an eyepiece micrometer. (**d**) Enzymatically dissociated IMR32- or primary NB-sphere cells were stained with trypan blue and counted to determine the number of viable cells.

the upregulation of CD133 (1.4-fold induction) and downregulation of RET receptors (5.9-fold reduction) were found in SFM medium, but not in the medium with 10% fetal bovine serum (Figure 5b). Next, we introduced CD133 into IMR32 cells by lentivirus infection, and after 5-week culture in SFM, we found that CD133-expressing cells formed many more large spheres than mock cells (Figure 5c). Moreover, CD133-expressing spheres made from IMR32 and primary NB cells contained many more living cells than the mock control (Figure 5d), suggesting that CD133 promotes NB cell survival in tumor-sphere formation.

Discussion

Increasing evidence highlights the function of CD133 as a marker of CSCs in various human tumors; however, its function in tumorigenesis remains to be elucidated by molecular biology experiments. In this study, CD133-knockdown experiments indicated that CD133 represses differentiation in NB cells; CD133 was clearly decreased by differentiation-inducing stimulation, for example ATRA and TPA treatments. Brodeur *et al.* (2000) indicated that neurotrophic factors and their receptors have a significant function in NB behavior and the potential to send intracellular signals into the nucleus to produce neuronal differentiation in the normal sympathetic nerve system. Among the NB cell differentiation-related neurotrophic receptors, *RET* transcription was regulated by CD133 in NB cell lines. The expression of CD133 effectively inhibited NB cell differentiation (neurite extension and differentiation markers). Furthermore, RET expression partly rescued the CD133-related inhibition of differentiation. These findings suggest that CD133-mediated RET suppression has a considerable function in NB cell differentiation. Regarding the function of RET in NB differentiation, Peterson and Bogenmann (2004) suggested that RET receptor activation inhibits cell cycle progression and enhances responsiveness to NGF; thus, NB cell differentiation requires the collaboration of functional RET and TrkA signal pathways; they also reported that GDNF treatment induced *RET* transcription in NB cells. Intriguingly, our results indicate that CD133 expression effectively suppressed *RET* mRNA in NB cells and CD133 knockdown induced NB cell differentiation, suggesting that suppression of CD133 by small-interference RNA administration will increase *RET* transcription in CD133-expressing NB tumors and may be useful in differentiation induction therapy for resistant- and relapsed-NB tumors. In addition, transcriptional suppression of *CD133* could be useful to induce differentiation in NB cells; however, the exact mechanism of transcriptional regulation of CD133 has not been clarified. Although seven CD133 mRNA isoforms controlled by five alternative promoters were reported previously (Shmelkov *et al.*, 2004), the promoter activities of these isoforms were studied only by pGL3-enhancer vector, suggesting the existence of other *cis*-elements in the CD133 locus.

Several studies have been reported to elucidate the molecular mechanism and signaling pathways that regulate the behavior of CD133-expressing cancer cells. Nikolova *et al.* (2007) reported that WNT-conditional media had effects on the proliferation and differentiation of cord blood-derived CD133-positive cells, and Fan *et al.* (2006) showed that Notch signal inhibition by GSI-18 reduced the CD133-positive fraction in brain tumor cells. Regarding the analysis of the intracellular signaling pathway related to the CD133 function, one report suggested the significance of the Akt/PKB pathway in the expression of survival proteins, phosphor-Bad and Bcl-2 in CD133-positive hepatocellular carcinoma cell survival (Ma *et al.*, 2007). In our study, CD133-knockdown experiments indicated that CD133-related RET repression and NB cell differentiation were caused by signal pathway activation, for example p38MAPK and PI3K/Akt pathways. To support this observation, treatment with kinase inhibitors showed a correlation between neurite elongation and RET induction in NB cells, and that differentiation marker protein induction was mainly dependent on the p38MAPK pathway. These findings suggest that CD133 prevents NB cell differentiation via signal transduction pathways. To the best of our knowledge, this is the first report of CD133-related signal pathway modification resulting in cell differentiation. As CD133 is a membranous protein on stem cells and cancer stem cells, it is possible that CD133 affects membranous receptor functions and the downstream signal pathways. In addition, Boivin *et al.* (2009) reported the phosphorylation of CD133-cytoplasmic tyrosine-828 and tyrosine-852 by Src and Fyn tyrosine kinases. Site-directed mutagenesis of these tyrosine residues in CD133 will provide important information for CD133 functions in our experimental system using NB cells.

Materials and methods

Cell culture and reagents

Human NB cell lines were obtained from official cell banks (RIKEN Cell Bank, Tsukuba, Japan and ATCC, Manassas, VA, USA) and cultured in high-glucose DMEM (Sigma-Aldrich, St Louis, MO, USA) or RPMI1640 (Wako, Osaka, Japan) supplemented with 10% heat-inactivated fetal bovine serum (Invitrogen, Carlsbad, CA, USA) and 50 μg/ml penicillin/streptomycin (Sigma-Aldrich) in an incubator with humidified air at 37 °C with 5% CO_2. NB cell lines subjected to molecular biology and biochemistry experiments were MYCN single-copy SH-SY5Y cells and MYCN-amplified TGW, SK-N-DZ and IMR32 cells. GDNF was obtained from Invitrogen. ATRA was from Sigma-Aldrich. Phorbol-12-myristate-13-acetate (TPA) was from Nacalai Tesque (Kyoto, Japan). LY294002 was from Cell Signaling Technology (Beverly, MA, USA). PD98059 and SB203580 were from Calbiochem (San Diego, CA, USA).

Fluorescence-activated cell sorting analysis

NB cell lines growing in the log phase were enzymatically removed from 10 cm diameter culture dishes, washed with cold PBS and treated with biotinylated AC133 (CD133/1) monoclonal antibodies (Miltenyi Biotec, Auburn, CA, USA) or control IgG2A (eBioscience, San Diego, CA, USA) for 15 min at 4 °C. The primary antibody was removed, and then the cells were washed twice with ice-cold PBS containing 0.1% BSA, and a 1:200 dilution of phycoerythrin-labeled streptavidin (eBioscience) added for 15 min at 4 °C. After washing, flow cytometry was performed using a fluorescence-activated cell sorting Caliber (BD, San Jose, CA, USA).

Knockdown of CD133

For RNAi experiments, predesigned, double-stranded SMART-pool small-interference RNA targeting human *CD133* (*prominin-1*) was purchased from Dharmacon (Lafayette, CO, USA) and Silencer Negative Control small-interference RNA #1 was purchased from Ambion (Austin, TX, USA).

Lentivirus-mediated gene transduction and knockdown

The packaging cell line HEK 293T (4×10^6) was plated and transfected the following day. Then, 1.5 μg transducing vectors containing the gene [pHR-SIN-CMV-G-DL1 or CSII-CMV-MCS-IRES2-Bsd vector (RIKEN Bioresource Center, Ibaraki, Japan)] or shRNA [pLKO.1 (Sigma-Aldrich)] and 2.0 μg packaging vectors (Sigma-Aldrich) were co-transfected with Fugene 6 transfection reagent (Roche Applied Science, Indianapolis, IN, USA) according to the manufacturer's protocols. The medium was changed the following day, and cells were cultured for another 24 h. Conditioned medium was collected and cleared of debris by filtering through a 0.45 μm filter (Millipore, Bedford, MA, USA). Then, 1×10^5 NB cells were seeded in each well of a six-well plate, and transduced by lentiviral-conditioned media. Transduced cells were analyzed by western blotting and RT–PCR.

Cloning of human CD133 cDNA

The human *CD133* cDNA (RefSeq NM_006017) was cloned from human colon cancer cell line Caco-2 mRNA by RT–PCR using specific primer sets described in Supplementary Table 1S. *CD133* cDNA fragment was sub-cloned into a lentiviral-based vector (pHR-SIN-CSGW) (Hasegawa *et al.*, 2006).

Western blot analysis

The cells were lysed in buffer containing 5 mM EDTA, 2 mM Tris–HCl (pH 7.5), 10 mM β-glycerophosphate, 5 μg/ml aprotinin, 2 mM phenylmethylsulfonyl fluoride, 1 mM Na_3VO_4, a protease inhibitor cocktail (Nacalai Tesque) and 1% SDS. Western blot analysis was performed as reported previously (Kurata *et al.*, 2008). For CD133 detection, we used AC133 monoclonal antibody. Anti-RET (Santa Cruz Biotechnology, Santa Cruz, CA, USA), anti-phospho- and total Akt, p38, ERK (Cell Signaling Technology) and anti-tubulin antibody from Lab Vision (Fremont, CA, USA) were also used.

Semi-quantitative RT–PCR

Semi-quantitative RT–PCR analysis was as described previously (Kurata *et al.*, 2008). Total cellular RNA for preparing RT–PCR templates was extracted using ISOGEN (Nippon Gene KK, Tokyo, Japan). The cDNA was synthesized from 1 μg total RNA and then subjected to PCR. Primer sequences are described in Supplementary Table 1S. RT–PCR results are representative of at least three independent experiments.

qPCR analysis

The qPCR analysis was performed as described previously (Ochiai *et al.*, 2010). The primers for qPCR were designed and synthesized to produce 50–150 bp products. The primer sequence is listed in Supplementary Table 1S. The results were representative of at least three independent experiments.

Cell proliferation and soft agar assay
Cells were seeded into 96-well plates (750 per well) in culture medium containing 10% fetal bovine serum. Every 24 h, cell viability was determined by water-soluble tetrazolium salt (WST-8) assay using Counting kit-8 (Dojindo, Kumamoto, Japan) according to the manufacturer's protocol. For soft agar assay, 2×10^3 cells of stable infectants TGW or SH-SY5Y cells were seeded in soft agar as described previously (Aoyama *et al.*, 2005). Viable colonies were stained with 0.05 mg/ml MTT.

Tumor formation in nude mice
For tumor formation, 6-week-old female athymic BALB/c AJcl *nu/nu* mice (CLEA Japan, Shizuoka, Japan) were injected into the femur with 1×10^7 TGW cells as described previously (Aoyama *et al.*, 2005). The handling of animals was in accordance with the guidelines of Chiba Cancer Center Research Institute.

Patients and tumor specimens
The 12 tumor specimens used in this study were kindly provided by various institutions and hospitals in Japan. Informed consent was obtained at each institution or hospital. All tumors were diagnosed clinically as well as pathologically as NB and staged according to the International NB Staging System criteria. The patients were treated by standard chemotherapy protocols as described previously (Kaneko *et al.*, 2002; Iehara *et al.*, 2006). *MYCN* copy number, *TrkA* mRNA expression levels and DNA index were measured as reported previously (Ohira *et al.*, 2003). This study was approved by the Institutional Review Board of Chiba Cancer Center.

Subcloning of human RET (RET9)
Human *RET9* (Crowder *et al.*, 2004) full-length cDNA was a kind gift from Dr Hideki Enomoto (RIKEN Center for Developmental Biology, Hyogo, Japan). *RET9* cDNA fragment (3.4 kb) was sub-cloned into the *Not*I site of CSII-CMV-MCS-IRES2-Bsd vector, which had been altered to accept the *Xba*I and *Hin*dIII ends.

Cloning of human RET promoter
Human *RET* promoter 1.5 kb (−919 to +550, position +1 is the transcription start site determined in a previous report (Itoh *et al.*, 1992)) was amplified from human genomic DNA using Platinum *Pfx* polymerase (Invitrogen) with primers (described in Supplementary Table 1S) by PCR amplification and sub-cloned into pGEM-T easy vector (Promega, Southampton, UK). The *RET* 5′-flanking sequence from −453 to +227 was sub-cloned into the *Eco*RV site of pGL4.17 reporter vector (Promega).

Sphere culture of NB cells
The preparation of primary NB cells from stage 4 patients' bone marrow was described previously (Nakanishi *et al.*, 2007). Dissociated primary NB cells or IMR32 cells were cultured in SFM (DMEM-F12, 1:1 (Wako), 50 μg/ml penicillin/streptomycin, 2% B27 supplement (Invitrogen), 20 ng/ml epidermal growth factor (Sigma-Aldrich) and 20 ng/ml fibroblast growth factor basic (Invitrogen)). Half of the medium was replaced with fresh culture medium every 7 days. IMR32 cells and primary NB cells were seeded in 96-well (400 per well) or six-well (1×10^5 per well) and six-well (1.7×10^5 per well) plates, respectively. Spheres were counted and measured under a microscope with an eyepiece micrometer. Five-week cultured IMR32 or 2-month cultured primary NB spheres were dissociated by Accumax (Innovative Cell Technologies, San Diego, CA, USA) according to the manufacturer's protocol. Living cells were counted based on morphological criteria and trypan blue staining.

Conflict of interest

The authors declare no conflict of interest.

Acknowledgements

We thank K Sakurai and S Matsushita for technical assistance, Dr Hiroyuki Miyoshi (BioResource Center, RIKEN) for the gift of CSII-CMV-MCS-IRES2-Bsd plasmid and Daniel Mrozek, Medical English Service, for editorial assistance. This work was supported in part by a grant-in-aid from JSPS for Young Scientists (B) (number: 19790274), a grant-in-aid from the Ministry of Health, Labor, and Welfare for Third Term Comprehensive Control Research for Cancer, a grant-in-aid for Cancer Research (20–13) from the Ministry of Health, Labor, and Welfare of Japan and a grant-in-aid from the Ministry of Education, Culture, Sports, Science and Technology, Japan (number: 21591377).

References

Aoyama M, Ozaki T, Inuzuka H, Tomotsune D, Hirato J, Okamoto Y *et al.* (2005). LMO3 interacts with neuronal transcription factor, HEN2, and acts as an oncogene in neuroblastoma. *Cancer Res* **65**: 4587–4597.

Boivin D, Labbé D, Fontaine N, Lamy S, Beaulieu E, Gingras D *et al.* (2009). The stem cell marker CD133 (prominin-1) is phosphorylated on cytoplasmic tyrosine-828 and tyrosine-852 by Src and Fyn tyrosine kinases. *Biochemistry* **48**: 3998–4007.

Brodeur GM, Sawada T, Tsuchida Y, Voute PA (eds) (2000). *Neuroblastoma*. Elsevier Science: Amsterdam.

Collins AT, Berry PA, Hyde C, Stower MJ, Maitland NJ. (2005). Prospective identification of tumorigenic prostate cancer stem cells. *Cancer Res* **65**: 10946–10951.

Corbeil D, Roper K, Hellwig A, Tavian M, Miraglia S, Watt SM *et al.* (2000). The human AC133 hematopoietic stem cell antigen is also expressed in epithelial cells and targeted to plasma membrane protrusions. *J Biol Chem* **275**: 5512–5520.

Corbeil D, Fargeas CA, Huttner WB. (2001). Rat prominin, like its mouse and human orthologues, is a pentaspan membrane glycoprotein. *Biochem Biophys Res Commun* **285**: 939–944.

Crowder RJ, Enomoto H, Yang M, Johnson Jr EM, Milbrandt J. (2004). Dok-6, a Novel p62 Dok family member, promotes Ret-mediated neurite outgrowth. *J Biol Chem* **279**: 42072–42081.

D'Alessio A, De Vita G, Cali G, Nitsch L, Fusco A, Vecchio G *et al.* (1995). Expression of the RET oncogene induces differentiation of SK-N-BE neuroblastoma cells. *Cell Growth Differ* **6**: 1387–1394.

Enomoto H, Crawford PA, Gorodinsky A, Heuckeroth RO, Johnson Jr EM, Milbrandt J. (2001). RET signaling is essential for migration, axonal growth and axon guidance of developing sympathetic neurons. *Development* **128**: 3963–3974.

Enomoto H, Heuckeroth RO, Golden JP, Johnson EM, Milbrandt J. (2000). Development of cranial parasympathetic ganglia

requires sequential actions of GDNF and neurturin. *Development* **127**: 4877–4889.

Fan X, Matsui W, Khaki L, Stearns D, Chun J, Li YM *et al.* (2006). Notch pathway inhibition depletes stem-like cells and blocks engraftment in embryonal brain tumors. *Cancer Res* **66**: 7445–7452.

Hansford LM, McKee AE, Zhang L, George RE, Gerstle JT, Thorner PS *et al.* (2007). Neuroblastoma cells isolated from bone marrow metastases contain a naturally enriched tumor-initiating cell. *Cancer Res* **67**: 11234–11243.

Hasegawa K, Nakamura T, Harvey M, Ikeda Y, Oberg A, Figini M *et al.* (2006). The use of a tropism-modified measles virus in folate receptor-targeted virotherapy of ovarian cancer. *Clin Cancer Res* **12**: 6170–6178.

Itoh F, Ishizaka Y, Tahira T, Yamamoto M, Miya A, Imai K *et al.* (1992). Identification and analysis of the *ret* proto-oncogene promoter region in neuroblastoma cell lines and medullary thyroid carcinomas from MEN2A patients. *Oncogene* **7**: 1201–1206.

Iehara T, Hosoi H, Akazawa K, Matsumoto Y, Yamamoto K, Suita S *et al.* (2006). MYCN gene amplification is a powerful prognostic factor even in infantile neuroblastoma detected by mass screening. *Br J Cancer* **94**: 1510–1515.

Jordan CT, Guzman ML, Noble M. (2006). Cancer stem cells. *N Engl J Med* **355**: 1253–1261.

Kaplan D, Matsumoto K, Lucarelli E, Thiele CJ. (1993). Induction of TrkB by retinoic acid mediates biologic responsiveness to BDNF and differentiation of human neuroblastoma cells. Eukaryotic Signal Transduction Group. *Neuron* **11**: 321–331.

Kaneko M, Tsuchida Y, Mugishima H, Ohnuma N, Yamamoto K, Kawa K *et al.* (2002). Intensified chemotherapy increases the survival rates in patients with stage 4 neuroblastoma with MYCN amplification. *J Pediatr Hematol Oncol* **24**: 613–621.

Klein R. (1994). Role of neurotrophins in mouse neuronal development. *FASEB J* **8**: 738–744.

Kurata K, Yanagisawa R, Ohira M, Kitagawa M, Nakagawara A, Kamijo T. (2008). Stress via p53 pathway causes apoptosis by mitochondrial Noxa upregulation in doxorubicin-treated neuroblastoma cells. *Oncogene* **27**: 741–754.

Ma S, Lee TK, Zheng BJ, Chan KW, Guan XY. (2007). CD133+ HCC cancer stem cells confer chemoresistance by preferential expression of the Akt/PKB survival pathway. *Oncogene* **27**: 1749–1758.

Maris JM, Hogarty MD, Bagatell R, Cohn SL. (2007). Neuroblastoma. *Lancet* **369**: 2106–2120.

Maw MA, Corbeil D, Koch J, Hellwig A, Wilson-Wheeler JC, Bridges RJ *et al.* (2000). A frameshift mutation in prominin (mouse)-like 1 causes human retinal degeneration. *Hum Mol Genet* **9**: 27–34.

Miki J, Furusato B, Li H, Gu Y, Takahashi H, Egawa S *et al.* (2007). Identification of putative stem cell markers, CD133 and CXCR4, in hTERT-immortalized primary nonmalignant and malignant tumor derived human prostate epithelial cell lines and in prostate cancer specimens. *Cancer Res* **67**: 3153–3161.

Monzani E, Facchetti F, Galmozzi E, Corsini E, Benetti A, Cavazzin C *et al.* (2007). Melanoma contains CD133 and ABCG2 positive cells with enhanced tumourigenic potential. *Eur J Cancer* **43**: 935–946.

Myers SM, Eng C, Ponder BA, Mulligan LM. (1995). Characterization of RET proto-oncogene 3′ splicing variants and polyadenylation sites: a novel C-terminus for RET. *Oncogene* **11**: 2039–2045.

Nakanishi H, Ozaki T, Nakamura Y, Hashizume K, Iwanaka T, Nakagawara A. (2007). Purification of human primary neuroblastomas by magnetic beads and their *in vitro* culture. *Oncol Rep* **17**: 1315–1320.

Nikolova T, Wu M, Brumbarov K, Alt R, Opitz H, Boheler KR *et al.* (2007). WNT-conditioned media differentially affect the proliferation and differentiation of cord blood-derived CD133+ cells *in vitro*. *Differentiation* **75**: 100–111.

O'Brien CA, Pollett A, Gallinger S, Dick JE. (2007). A human colon cancer cell capable of initiating tumour growth in immunodeficient mice. *Nature* **445**: 106–110.

Ochiai H, Takenobu H, Nakagawa A, Yamaguchi Y, Kimura M, Ohira M *et al.* (2010). Bmi1 is a MYCN target gene that regulates tumorigenesis through repression of *KIF1Bβ* and *TSLC1* in neuroblastoma. *Oncogene* **29**: 2681–2690.

Ohira M, Morohashi A, Inuzuka H, Shishikura T, Kawamoto T, Kageyama H *et al.* (2003). Expression profiling and characterization of 4200 genes cloned from primary neuroblastomas: identification of 305 genes differentially expressed between favorable and unfavorable subsets. *Oncogene* **22**: 5525–5536.

Olempska M, Eisenach PA, Ammerpohl O, Ungefroren H, Fandrich F, Kalthoff H. (2007). Detection of tumor stem cell markers in pancreatic carcinoma cell lines. *Hepatobiliary Pancreat Dis Int* **6**: 92–97.

Peterson S, Bogenmann E. (2004). The RET and TRKA pathways collaborate to regulate neuroblastoma differentiation. *Oncogene* **23**: 213–225.

Reya T, Morrison SJ, Clarke MF, Weissman IL. (2001). Stem cells, cancer, and cancer stem cells. *Nature* **414**: 105–111.

Ricci-Vitiani L, Lombardi DG, Pilozzi E, Biffoni M, Todaro M, Peschle C *et al.* (2007). Identification and expansion of human colon-cancer initiating cells. *Nature* **445**: 111–115.

Shmelkov SV, Jun L, St Clair R, McGarrigle D, Derderian CA, Usenko JK *et al.* (2004). Alternative promoters regulate transcription of the gene that encodes stem cell surface protein AC133. *Blood* **103**: 2055–2061.

Singh SK, Hawkins C, Clarke ID, Squire JA, Bayani J, Hide T *et al.* (2004). Identification of human brain tumour initiating cells. *Nature* **432**: 396–401.

Walton JD, Kattan DR, Thomas SK, Spengler BA, Guo HF, Biedler JL *et al.* (2004). Characteristics of stem cells from human neuroblastoma cell lines and in tumors. *Neoplasia* **6**: 838–845.

Weinberg RA (ed) (2006). *The Biology of Cancer*. Garland Science: New York.

Yin AH, Miraglia S, Zanjani ED, Almeida-Porada G, Ogawa M, Leary AG *et al.* (1997). AC133, a novel marker for human hematopoietic stem and progenitor cells. *Blood* **90**: 5002–5012.

Yin S, Li J, Hu C, Chen X, Yao M, Yan M *et al.* (2007). CD133 positive hepatocellular carcinoma cells possess high capacity for tumorigenicity. *Int J Cancer* **120**: 1444–1450.

Zacchigna S, Oh H, Wilsch-Bräuninger M, Missol-Kolka E, Jászai J, Jansen S *et al.* (2009). Loss of the cholesterol-binding protein prominin-1/CD133 causes disk dysmorphogenesis and photoreceptor degeneration. *J Neurosci* **29**: 2297–2308.

Supplementary Information accompanies the paper on the Oncogene website (http://www.nature.com/onc)

MOLECULAR AND CELLULAR BIOLOGY, Jan. 2011, p. 351–364 Vol. 31, No. 2
0270-7306/11/$12.00 doi:10.1128/MCB.00259-10

Mammalian Polycomb-Like Pcl2/Mtf2 Is a Novel Regulatory Component of PRC2 That Can Differentially Modulate Polycomb Activity both at the *Hox* Gene Cluster and at *Cdkn2a* Genes▽

Xiangzhi Li,[1] Kyo-ichi Isono,[1]† Daisuke Yamada,[1]† Takaho A. Endo,[2] Mitsuhiro Endoh,[1,3] Jun Shinga,[1] Yoko Mizutani-Koseki,[1] Arie P. Otte,[4] Miguel Casanova,[5] Hiroshi Kitamura,[1] Takehiko Kamijo,[6] Jafar Sharif,[1] Osamu Ohara,[1] Tetsuro Toyada,[2] Bradley E. Bernstein,[7] Neil Brockdorff,[5] and Haruhiko Koseki[1,3]*

RIKEN Research Center for Allergy and Immunology[1] and RIKEN Bioinformatics and Systems Engineering Division,[2] 1-7-22 Suehiro, Tsurumi-ku, Yokohama 230-0045, Japan; JST, CREST, 1-7-22 Suehiro, Tsurumi-ku, Yokohama 230-0045, Japan[3]; Swammerdam Institute for Life Sciences, University of Amsterdam, Kruislaan 406, 1098 SM Amsterdam, Netherlands[4]; Department of Biochemistry, University of Oxford, South Parks Road, Oxford OX1 3QU, United Kingdom[5]; Division of Biochemistry, Chiba Cancer Center Research Institute, 666-2 Nitona, Chuoh-ku, Chiba 260-8717, Japan[6]; and MGH Pathology, Harvard University, 185 Cambridge Street, Boston, Massachusetts 02114[7]

Received 8 March 2010/Returned for modification 17 April 2010/Accepted 23 October 2010

The Polycomb group of proteins forms at least two distinct complexes designated the Polycomb repressive complex-1 (PRC1) and PRC2. These complexes cooperate to mediate transcriptional repression of their target genes, including the *Hox* gene cluster and the *Cdkn2a* genes. Mammalian Polycomb-like gene Pcl2/Mtf2 is expressed as four different isoforms, and the longest one contains a Tudor domain and two plant homeodomain (PHD) fingers. Pcl2 forms a complex with PRC2 and binds to *Hox* genes in a PRC2-dependent manner. We show that Pcl2 is a functional component of PRC2 and is required for PRC2-mediated *Hox* repression. Pcl2, however, exhibits a profound synergistic effect on PRC1-mediated *Hox* repression, which is not accompanied by major alterations in the local trimethylation of histone H3 at lysine 27 (H3K27me3) or PRC1 deposition. Pcl2 therefore functions in collaboration with both PRC2 and PRC1 to repress *Hox* gene expression during axial development. Paradoxically, in embryonic fibroblasts, Pcl2 is shown to activate the expression of *Cdkn2a* and promote cellular senescence, presumably by suppressing the catalytic activity of PRC2 locally. Taken together, we show that Pcl2 differentially regulates Polycomb-mediated repression of *Hox* and *Cdkn2a* genes. We therefore propose a novel role for Pcl2 to modify functional engagement of PRC2 and PRC1, which could be modulated by sensing cellular circumstances.

The Polycomb group (PcG) was first identified in *Drosophila melanogaster* as a gene cluster necessary for the maintenance of segmental identity (50, 53). The PcG proteins are required for the epigenetic repression of a number of developmental regulatory genes, including homeotic genes. They do so by forming at least two distinct multimeric protein complexes at their target loci, known as Polycomb repressive complex-1 (PRC1) and PRC2 (11, 13, 46, 57).

In *Drosophila*, the core PRC1 is formed by four proteins, Polycomb (Pc), Polyhomeotic (Ph), Posterior sex combs (Psc), and dRing (Sex comb extra; Sce), which inhibit the chromatin remodeling activity of SWI/SNF complexes (20, 35). Mammalian orthologs form functionally similar complexes (40). PRC1 has been shown to act as an E3 component for ubiquitination of histone H2A at lysine 119 (uH2A) via Ring1B and Ring1A catalytic subunits (9, 14, 62). In addition, regulation of higher-order chromatin structure is a recently identified function mediated by PRC1 (19). The core of the mammalian PRC2 is composed of three evolutionarily conserved proteins, Eed, an ortholog of extra sex combs [Esc]), Ezh2, an ortholog of enhancer of zeste [E(z)], and Suz12, which mediates trimethylation of histone H3 at lysine 27 by the Ezh2 component (11, 13, 46, 48, 51, 60). Although both PRC1 and PRC2 are required to maintain *Hox* repression and share target loci in both vertebrates and invertebrates, these complexes do not associate with each other in most cell types. A plausible model for Polycomb silencing is through the engagement of PRC1 with the target via its interaction with H3K27me3 mediated by the chromodomain of Pc or its mammalian counterparts (11, 62). However, recent genome-wide analysis of PRC1 and PRC2 occupancy revealed that PRC1 binding demarcated a portion of the PRC2 targets (37), implying that functional engagement of PRC1 and PRC2 is not constitutive but, instead, is regulated by undefined intrinsic and/or extrinsic signals.

The *polycomblike* (*Pcl*) gene was initially isolated as a PcG gene during a *Pc* mutation modifier screen in *D. melanogaster* and then identified in several studies as an enhancer

* Corresponding author. Mailing address: RIKEN Research Center for Allergy and Immunology, 1-7-22 Suehiro, Tsurumi-ku, Yokohama 230-0045, Japan. Phone: 81 45 503 9689. Fax: 81 45 503 9688. E-mail: koseki@rcai.riken.jp.
† K.-I.I. and D.Y. contributed equally to this work.
▽ Published ahead of print on 8 November 2010.

TABLE 1. Antibodies used in this study

Specificity	Species	Antibody type	Source or reference	Catalog or clone no.
Pcl2	Mouse	Monoclonal	This paper	3A9
Pcl2	Rabbit	Antiserum	This paper	
Rnf2	Mouse	Monoclonal	5	Clone 3
Phc2	Mouse	Monoclonal	28	4G9
Mel18	Goat	Antiserum	Santa Cruz (Santa Cruz, CA)	C-20
Mel18	Rabbit	Antiserum	Santa Cruz (Santa Cruz, CA)	H-115
Eed	Mouse	Monoclonal	23	M26
Ezh2	Mouse	Monoclonal	23	M10
Ezh2	Rabbit	Monoclonal	Upstate (Lake Placid, NY)	07-400
Suz12	Rabbit	Antiserum	Upstate (Lake Placid, NY)	07-379
Histone H3K27me3	Rabbit	Antiserum	Upstate (Lake Placid, NY)	07-449
Histone H3K4me3	Rabbit	Antiserum	Upstate (Lake Placid, NY)	07-473
Histone H2Aub1	Mouse	Monoclonal	Upstate (Lake Placid, NY,)	E6C5
FLAG	Mouse	Monoclonal	Sigma-Aldrich (St. Louis, MO)	F-3165
Myc	Mouse	Monoclonal	Upstate (Lake Placid, NY)	4A6
γ-Tubulin	Rabbit	Antiserum	Sigma-Aldrich (St. Louis, MO)	T3320
$p19^{ARF}$	Rabbit	Antiserum	Abcam (Cambridge, UK)	R562
$p16^{ink4a}$	Rat	Monoclonal	NeoMarkers (Fremont, CA)	16P04

for *Esc* mutations (17, 33). *Pcl* mutant phenotypes are similar to those of *Pc* mutants, and interactions between mutant *Pcl* and *Pc* or *Esc* synergistically enhance the respective phenotypes in a dose-dependent manner. The Pcl protein has a Tudor domain and two tandem plant homeodomain (PHD) fingers (43, 49, 64). Pcl has been shown to be a part of two distinct protein complexes, PRC2 and a thus far uncharacterized complex, which appear at *Drosophila* embryonic and larval stages, respectively (47, 56, 61). In *Drosophil*a embryos, Pcl forms complexes with PRC2 and maximizes its catalytic activity at Polycomb target genes (47). In the larval stage, although Pcl does not form complexes with PRC2, it mediates pleiohomeotic-dependent PRC2 target binding (56). These findings imply that Pcl plays at least two distinct roles in regulating the expression of Polycomb targets by interacting with different protein complexes and suggest that these interactions depend on the developmental stage or cell type. The picture may be even more complex because functional interactions of Pcl could potentially extend to PRC1. In addition, Pcl has been shown to display extensive colocalization with Pc and Polyhomeotic (Ph) proteins on the polytene chromosomes (43), and genetic interactions between *Pcl* and *Pc* have also been demonstrated (33). These observations suggest that Pcl may have multiple regulatory functions in mediating Polycomb repression.

Three homologs of the *Drosophila Pcl* gene have been identified in vertebrates, frogs, chickens, and mammals and are named, *Pcl1* (also *Phf1* or *tctex3*), *Pcl2*/*Mtf2* (also *M96*; here, designated *Pcl2*) and *Pcl3* (also *Phf19*) (12, 27, 32, 36, 64, 66). Overexpression studies using *Xenopus* and chicken embryos demonstrated that Pcl1 and/or Pcl2 mediates the repression of developmental regulatory genes such as *En-2*, *Krox20*, *Hoxb9*, and *Shh* (36, 64, 66). Murine and human orthologs of these genes have been shown to be the targets of PRC1 and PRC2 as revealed by genome-wide chromatin immunoprecipitation (ChIP) assays (8, 38). These findings imply that vertebrate as well as *Drosophila* Pcl family proteins may be part of the PcG complex. In support of this idea, hPHF1 was copurified with a subset of PRC2 and was shown to enhance the catalytic activity of PRC2 in a human cell line (10, 55). Unexpectedly, however, hPHF1 was also found to form complexes with proteins involved in the DNA damage response (25). Despite these recent advances, the molecular basis underlying the multiple functions of Pcl family proteins is not well understood. Although the biochemical properties of hPHF1 have been elucidated, a genetic approach using loss-of-function mutants of the mammalian *Pcl* family is still needed to clarify the genetic cascades involving the Pcl orthologs. A study using a *Pcl2* gene trap allele suggested the involvement of Pcl2 in anterior-posterior (A-P) specification of the axis (63); however, the mechanistic basis of the involvement remains unclear. To address these questions, we have combined genetic and biochemical approaches to clarify the role of Pcl2 in Polycomb-mediated repression at the *Hox* gene cluster and *Cdkn2a* genes.

MATERIALS AND METHODS

Determination of *Pcl2* gene structure. Data sets of RNA-Seq experiments performed by Motazavi et al. (45) were downloaded (http://woldlab.caltech.edu/~alim/RNAseq/). Results from two biological replicates were summed for three cell types (brain, liver, and muscle). Positions of the 15 *Pcl2* exons (*Mtf2* in the database) were identified using the BLASTN (3) program with *Mtf2* as the reference sequence (GenBank accession number NM_013827.2) and mouse chromosome 5 (NCBI version 37) (see Fig. S1A posted at http://web.rcai.riken.jp/en/paper_figs/Li_Supp_figs_rev3.pdf).

Production of anti-Pcl2 monoclonal antibody (MAb) and antiserum. A partial cDNA fragment that included the PHD fingers (amino acids [aa] 103 tp 327) of Pcl2 was isolated by yeast two-hybrid screening for Mel18-interacters and subcloned into the pGEX-4T-3 vector (Amersham Biosciences) to express a glutathione *S*-transferase (GST)-Pcl2 fusion protein. This fusion protein was used to generate hybridomas as described previously (29). Rabbit polyclonal antiserum was raised against a synthetic polypeptide corresponding to amino acids 20 to 36 of Pcl2 (RNQKTSASLNKLSLQDGC) conjugated to keyhole limpet hemocyanin. A purified IgG fraction of this antiserum was used for immunoprecipitation (IP) and immunofluorescence.

Immunoprecipitation, Western blot analyses, and gel filtration chromatography. IP and Western blot analyses were performed as described previously (28). Antibodies used in this study are listed in Table 1 (5, 23, 28). Nuclear proteins were extracted from nuclear pellets of K562 cells as described previously (15). Nuclear extracts were loaded onto Superose 6 columns (Amersham Biosciences), and 0.5-ml fractions were collected. Proteins from each fraction were concentrated by trichloroacetic acid-deoxycholate precipita-

TABLE 2. PCR primers used in this study

Primer function	Name	Primer sequence	
		Forward	Reverse
ChIP	Hoxa4	AGCTCCAGCCCTGGCTTCGC	CGTGATGGATGCTGCTAGCC
	Hoxb4	AAACCGAGTCAAGGGGTCGG	CGCGTAGCGCTGCACAGTGC
	Hoxb6	CCGCATAGCCAGACGAGTAG	CTGCCTCTGCCATTGGTCAG
	Hoxb8	TGGAGCTGGAGAAGGAGTTCCTA	CAGAAGCTATTACGAGATACTACC
	Hprt	CTCCTAAGGTTACTAAGTAG	CAAAGGCAGTTCCGGAACTC
	Ink4a	CTACAGAAGAGATGCAGGGTTC	AAGGAGAGATTTCGAGAAGGAC
	Actin	CTACACGCTAGGCGTAAAGTTG	TCTCGTGGCTAGTACCTCACTG
RT-PCR	Hoxa1	AGATGGACAATGCAAGAATG	TCAGTGGGAGGTAGTCAGAG
	Hoxb3	ACCTACTACGACAACACCGC	TGCGACGGTTCTGGAACCAG
	Hoxb4	GATCAACTCAAACTATGTCG	TGGTGTTGGGCAACTTGTGG
	Hoxb6	GTTCCTATTTCGTGAACTCC	AGCACCTTCACTCGGCTGGC
	Hoxb8	GGAGAGGAAGCTGTATGATC	GATATCTCTTGCCTCACAAC
	Hprt	ATGAGTACTTCAGGGATTTG	TGGCCTATAGGCTCATAGTG
	Arf	CTTGGTCACTGTGAGGATTCAG	CTATGCCCGTCGGTCTGGGC
	Ink4a	TCCGCTGCAGACAGACTGGCCAG	CTATGCCCGTCGGTCTGGGC
Genotyping	$Pcl2^{WT}$	GATGGTCAGATGGCTTGTTT	AGGTAGGTAAGTGGTGGTGC
	$Pcl2^{GT}$	GATGGTCAGATGGCTTGTTT	CAAGGCGATTAAGTTGGGTAACG
	$Pcl2^{\Delta}$	GGAACTCACTCTGTAGACCCTT	CAATGCTGGGTAGGCTGA

tion. Equal amounts of each sample were run on SDS-PAGE gels and subjected to Western blot analysis.

Generation of *Pcl2* mutant mice and ES cells. The gene-trapped embryonic stem (ES) cell line for the *Pcl2* locus (M016A06) was obtained from the European Mouse Mutant Archive (24). The endogenous *Pcl2* locus was disrupted by the insertion of a retroviral U3 β-galactosidase–Neo^r fusion gene (β-geo) gene trap vector. Its insertion into exon 4 results in disruption of the *Pcl2* open reading frame (ORF) (see Fig. S2 posted at http://web.rcai.riken.jp/en/paper_figs/Li_Supp_figs_rev3.pdf).

To generate deletion mutant mice, *Pcl2* homology arms, a 3.4-kb XbaI fragment that lies at the 5′ end of the exon 4 and a 2.4-kb KpnI/SalI fragment encompassing part of exon 5, were first introduced into the pPNT-loxP-Neo vector, in which the neomycin resistance gene (Neo^r) cassette was placed between two *loxP* sites (see Fig. S3 posted at the URL mentioned above). Homologous recombinants and germ line chimeras were isolated as described previously (1) (see Fig. S3B posted at the URL mentioned above). Heterozygous mutants were bred with CAG-Cre transgenic mice to delete the Neo^r cassette (54). $Pcl2^{+/\Delta}$ mice were backcrossed six times onto a C57BL/6 background. $Pcl2^{+/\Delta}$ mice were crossed with $Phc2^{+/-}$, $Mel18^{+/-}$, and $Suz12^{+/-}$ mice to generate compound mutants. All animal experiments were carried out according to the in-house guidelines for the care and use of laboratory animals of the RIKEN, Yokohama Institute, Japan.

Homozygous mutant ES cells were derived from respective mutant embryos as described previously (14). Primer pairs used for genotyping of these mutant alleles are listed in Table 2.

ChIP analysis. ChIP analysis was performed as described previously (18, 29). The primers used in this study are listed in Table 2.

ChIP-chip and ChIP-seq analyses. We used Agilent Mouse Promoter ChIP-on-Chip Set 244K with chromatin immunoprecipitation (ChIP-chip) using antibodies against H3K27me3, Ring1B, or Pcl2. We used probes showing significant intensities above background ($P < 10^{-7}$, Student's t test) and located from −4 kb to +4 kb of the transcription start site (TSS) of mouse genes. Methylated, ubiquitinated, or Ring1B- or Pcl2-binding positions were defined where the signal intensity of ChIP was 4 times (H3K27me3 and Pcl2) or 10 times (Ring1B) greater than that of input and when the statistical significance between the signals was less than 10^{-3}. To reduce noise in these assays, we removed detected probes that did not have significantly strong signals from input around the 500-bp region flanking their respective positions. ChIP followed by high-throughput sequencing (ChIP-seq) analysis was performed as described previously (37). Since this study is aimed to specifically elucidate the role of Pcl2 at the *Hox* and *Cdkn2a* genes, whole data sets of these analyses will be published elsewhere.

Skeletal, *in situ* RNA, and real-time PCR analyses. Skeletal preparations were made from perinatal mice, and cleared skeletons were analyzed under a stereomicroscope as described previously (1). *In situ* hybridization of tissue sections was performed as described previously (1). RNA extraction from ES cells, reverse transcription, and PCRs were performed as described previously (21). The expression of *Hox* and *Tbx3* genes was quantified relative to *Hprt* expression by real-time PCR analyses using an Mx3005P multiplex quantitative PCR system (Stratagene). Primer pairs used for reverse transcription-PCR (RT-PCR) analysis are listed in Table 2.

Cell culture of primary MEFs. Mouse embryonic fibroblasts (MEFs) were prepared as described previously (31). The *Mel18*-null, *Mel18/ARF*, and *Mel18/p53* double-null MEFs were routinely maintained with Dulbecco's modified Eagle's medium (DMEM) supplemented with 20% fetal bovine serum (FBS), 1× nonessential amino acids (Invitrogen), and 1× penicillin-streptomycin (Invitrogen). In modified 3T9 assays, cells were passaged at 3-day intervals and counted after trypsinization, and the number of cells per dish was recorded. A total of 1×10^6 cells were replated in 60-mm diameter dishes every 3 days (31). In growth rate assays, cells diluted to 2×10^4 cells per 60-mm diameter dish were plated in duplicate, and thereafter individual cultures harvested each day were counted. The Pcl2 expression retrovirus was prepared using a retrovirus packaging system (PlatE), according to the manufacturer's instructions, and transduced into immortalized MEF $Pcl2^{GT/GT}$ cells.

RESULTS

Identification of *Pcl2* transcripts and their products. Using database screening (GenBank accession number NM_013827.2), we identified a *Pcl2* transcript that is predicted to encode a protein containing a Tudor domain, two PHD fingers in the N-terminal region, and a chromo-like domain structure in the C-terminal region (Fig. 1A, upper scheme). In addition, we found a shorter transcript encoding a protein (AAI00341.1) lacking the Tudor domain (Fig. 1A, lower scheme). To elucidate the origin of the *Pcl2* isoforms, we examined the promoter and exon usage at the *Pcl2* locus through data sets obtained from recent genome-wide analyses for H3K4me3 occupancy and RNA transcription (see Fig. S1A posted at http://web.rcai.riken.jp/en/paper_figs/Li_Supp_figs_rev3.pdf) (44, 45). *Pcl2* appears to have a single predominant transcription start site, where there is extensive H3K4 trimethylation. We further found that usage of the 15 *Pcl2* exons was not necessarily uniform and that exons 2, 3, 5, and 11 were differentially expressed among brain, liver, and muscle. This analysis suggests that the *Pcl2*

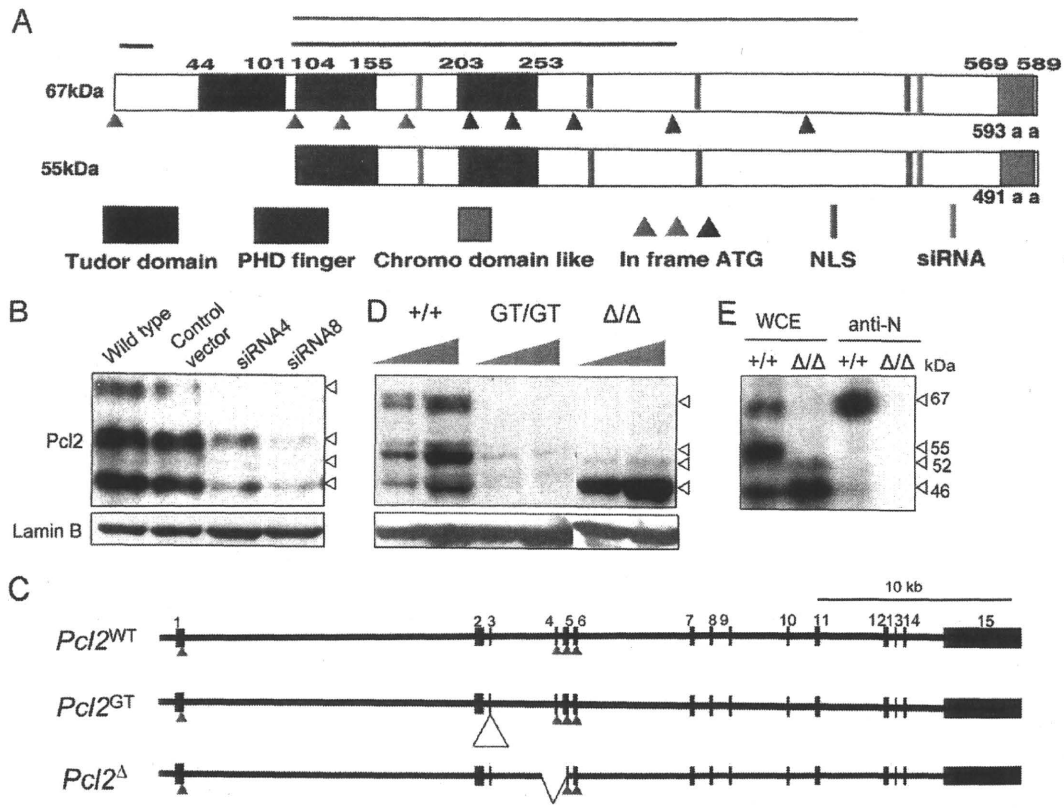

FIG. 1. Primary structure and the expression of mouse Pcl2 gene products. (A) Schematic representation of the two predicted Pcl2 isoforms. The black box corresponding to aa 44 to 101 representing the Tudor domain. The two dark blue boxes represent the PHD fingers. Three red vertical bars delineate the putative nuclear localization signals (NLS). A light blue box at aa 569 to 589 shows the chromo-like domain region at the C terminus. Positions for siRNA are demonstrated by light blue bars. The cDNA fragment isolated by two-hybrid screening for Mel18 interacting factors is shown by a green line at the top. The peptide and the fragment used to generate anti-Pcl2 antibodies are represented by two black lines. All ATG codons in the correct reading frame are indicated by colored triangles. Putative translation initiation codons for the 67- and 55-kDa isoforms are demarcated by red triangles, and those for 52- and 46-kDa isoforms are indicated by green triangles. (B) Expression of multiple Pcl2 isoforms in ES cells. The 67-, 55-, 52-, and 46-kDa bands were detected on Western blots of whole-cell lysates from wild-type ES cells using the Pcl2 MAb. The expression of *Pcl2* siRNA proportionally reduced the intensity of all four bands, whereas they were unaffected by the control siRNA. Lamin was used as a loading control. (C) Schematic representation of the genomic organization of $Pcl2^{GT}$ and $Pcl2^{\Delta}$ alleles. The $Pcl2^{GT}$ allele resulted from insertion of a gene trap vector (indicated by an open triangle) into exon 3. In the $Pcl2^{\Delta}$ allele, the genomic region encompassing the fourth intron to the middle of exon 5 is deleted. Genomic positions for putative translation initiation codons for the 67- and 55-kDa isoforms are indicated by red triangles, and those for 52- and 46-kDa isoforms are indicated by green triangles. (D) The 67-, 55-, 52-, and 46-kDa bands detected by the Pcl2 MAb were absent in $Pcl2^{GT/GT}$ ES cells, whereas only the 67- and 55-kDa bands were affected in $Pcl2^{\Delta/\Delta}$ ES cells. (E) Polyclonal antibodies against the N-terminal peptide of Pcl2 (anti-N) exclusively immunoprecipitated the 67-kDa isoform in the wild-type ES cells. WCE, whole-cell extract. The blot was probed with the Pcl2 MAb.

locus can give rise to several different transcripts, most likely due to alternative exon usage. We therefore inferred that the Pcl2 isoform lacking the Tudor domain could be produced from a transcript possessing exons 2 and 3 (see Fig. S1B posted at the URL mentioned above). In this case the nascent peptide initiating at the exon 1 start codon would prematurely terminate because of a frameshift; instead, productive translation would initiate at the start codon in exon 4, giving rise to a protein equivalent to AAI00341.1 (indicated by a green triangle in Fig. S1B posted at the URL mentioned above).

We then used Western blot analysis using a MAb produced against a GST-Pcl2 (aa 103 to 327) fusion protein to examine the expression of Pcl2 gene products. The MAb reproducibly detected strong bands of 67, 55, and 46 kDa and a much weaker 52-kDa band in whole-cell extracts of wild-type ES cells (Fig. 1B). To clarify whether these bands represent isoforms of Pcl2, we measured the effect of small interfering RNA (siRNA)-mediated knockdown of *Pcl2* in ES cells (Fig. 1A) on the appearance of the bands. Expression of two different siRNA constructs reduced the intensity of all four bands proportionally (Fig. 1B). These data indicate that *Pcl2* is expressed primarily as 67-, 55-, 52-, and 46-kDa isoforms.

To further elucidate the origin of the Pcl2 isoforms, we used two mutant alleles for *Pcl2*. Insertion of a gene-trap vector into exon 3 ($Pcl2^{GT}$) is expected to impair the expression of Pcl2 (Fig. 1C; see also Fig. S2 posted at http://web.rcai.riken.jp/en/paper_figs/Li_Supp_figs_rev3.pdf). In $Pcl2^{GT/GT}$ ES cells, we found this insertion diminished band intensities (Fig. 1D). In another allele, we deleted exon 4 and part of exon 5 by targeted mutagenesis ($Pcl2^{\Delta}$) (Fig. 1C; see also Fig. S3 posted at the URL mentioned above). This deletion resulted in the expression of truncated *Pcl2* transcripts in which exon 4 and 5 were skipped (X. Li, unpublished observations). These truncated

transcripts are predicted to encode a Pcl2 protein lacking the Tudor domain and the first PHD finger. Consistent with this prediction, the 67- and 55-kDa bands were abolished in $Pcl2^{\Delta/\Delta}$ ES cells. Therefore, the 67- and 55-kDa isoforms represent proteins with and without the Tudor domain, respectively (Fig. 1A). To validate this interpretation, we generated a polyclonal antibody against a synthetic polypeptide corresponding to part of the Pcl2 Tudor domain (aa 20 to 36). This antibody exclusively immunoprecipitated the 67-kDa band, confirming the presence of the Tudor domain in this isoform (Fig. 1E).

***Hox* repression by Pcl2.** *Hox* cluster genes are evolutionarily conserved targets for Polycomb repression during A-P specification of the axis. We thus examined axial skeletal development in $Pcl2^{GT/GT}$ and $Pcl2^{\Delta/\Delta}$ mice. Both mutant mice survived to birth; however, most of the $Pcl2^{GT/GT}$ mice died before weaning. In contrast, $Pcl2^{\Delta/\Delta}$ mice were viable and fertile. Although postnatal viabilities of the $Pcl2^{GT/GT}$ and $Pcl2^{\Delta/\Delta}$ mice were different, similar axial skeletal alterations that are characteristic of posterior transformations were observed in both mutants, as shown in a previous study (65) (Fig. 2A and B). Briefly, ectopic ribs that associated with the seventh cervical vertebra (C7) were frequently seen in $Pcl2^{GT/GT}$ and $Pcl2^{\Delta/\Delta}$ mice (indicated by arrows in Fig. 2A, frames b, c, e, f, n, and o). Consistent with this malformation, sternums were shifted anteriorly (indicated by brackets in Fig. 2A, frames b and c). The odontoid process, which is normally a characteristic of the second cervical vertebra (C2), was frequently associated with the first cervical vertebra (C1) in the mutants (indicated by red triangles in Fig. 2A, frames h to j). Axial skeletal changes indicating posterior transformations were also manifested at thoracolumbar and lumbosacral transitions of $Pcl2^{GT/GT}$ and $Pcl2^{\Delta/\Delta}$ mice (Fig. 2B). Therefore, Pcl2 proteins, particularly the 67- and/or 55-kDa isoforms, are required for A-P specifications of the axis, similar to other PcG proteins.

Next, we used *in situ* hybridization analysis to determine whether homeotic transformations in $Pcl2^{\Delta/\Delta}$ mice were accompanied by *Hox* gene derepression. The anterior boundaries of *Hoxb4*, *Hoxb6*, *Hoxb8*, and *Hoxd4* expression in the developing sclerotome were shifted cranially in $Pcl2^{\Delta/\Delta}$ embryos at 11.5 days postcoitus (dpc) (Fig. 2C). These results are consistent with homeotic transformations in the cervical and cervicothoracic boundary regions. We also found subtle but significant derepression of several *Hox* genes in $Pcl2^{\Delta/\Delta}$ ES cells (Fig. 2D). These results show that Pcl2 regulates *Hox* gene expression.

Pcl2 binds to *Hox* genes in a PRC2-dependent manner. Recent chromatin immunoprecipitation (ChIP) analyses revealed deposition of PRC2, PRC1, and H3K27me3 at the *Hox* cluster in developing embryos and ES cells. In parallel, *Drosophila* Pcl and human PHF1 were shown to be included in PRC2 in *Drosophila* and human cells, respectively (10, 47, 55, 56). Moreover, ChIP-seq studies reported significant overlap of genes bound by Pcl2 and Ezh2 in ES cells (41). These observations prompted us to hypothesize that Pcl2 mediates *Hox* repression via direct association with the *Hox* genes. By conventional ChIP assay using an anti-Pcl2 polyclonal antibody, we immunoprecipitated promoter regions of *Hoxb4*, *Hoxb6*, and *Hoxb8* from the wild-type ES cells but not from $Pcl2^{\Delta/\Delta}$ ES cells, which were used as a negative control (Fig. 3A). This result was further validated by ChIP-chip analysis using $Pcl2^{GT/GT}$ ES cells, which are reconstituted with the 67-kDa isoform of myc-tagged Pcl2. Here, an anti-myc antibody was used instead of the polyclonal antibody against the N-terminal peptide of Pcl2 (anti-N). In this experiment, too, we found considerable Pcl2 deposition around the transcription start sites (TSSs) of the *Hox* gene cluster, all of which were cooccupied by H3K27me3 and Ring1B (Fig. 3B; also D. Yamada and H. Koseki, unpublished data). Based on these results, we extended our analyses to the entire *Hoxd* cluster by ChIP-seq analysis using the anti-Pcl2 polyclonal antibody (Fig. 3C) (37). Indeed, the distribution profile of Pcl2 at the *Hoxd* cluster was similar to that of both Ezh2 and Ring1B. In particular, clear peaks that represented extensive binding of Pcl2, Ezh2, and Ring1B appeared concurrently around *Hoxd9*, *Hoxd10*, *Hoxd11*, *Hoxd12*, *Hoxd13*, and *Evx2*. Therefore, Pcl2 binds to *Hox* cluster genes, and its binding is correlated with local depositions of PRC2 and PRC1.

We went on to test whether Pcl2 expression and target binding depend on PRC2 because the expression of PRC2 components is known to be mutually dependent, and Pcl2 has already been reported as a PRC2-associated protein in mouse ES cells (21, 41, 63) (see Fig. S4 posted at http://web.rcai.riken.jp/en/paper_figs/Li_Supp_figs_rev3.pdf). In agreement with this view, we observed that the expression of Pcl2, as well as of Eed and Ezh2, was considerably decreased in $Suz12^{-/-}$ ES cells (Fig. 3D) (21). Particularly, the 67- and 55-kDa isoforms of Pcl2 were almost absent. We further used ChIP assays to confirm this result. Consistent with the reduction of Pcl2 expression in $Suz12^{-/-}$ ES cells, Pcl2 binding was almost nonexistent (Fig. 3E). It is worth noting that level of *Pcl2* transcripts was not proportionally altered in comparison to that of Pcl2 proteins in $Suz12^{-/-}$ ES cells (Fig. 3F). This suggests that Pcl2 expression is posttranscriptionally regulated in a PRC2-dependent manner. In contrast, the expression of Pcl2 and its binding to *Hox* genes were unaffected in $Ring1B^{-/-}$ ES cells (Fig. 4A and B). Moreover, the expression of PRC2 and PRC1 and their binding to *Hox* genes were not affected in $Pcl2^{\Delta/\Delta}$ ES cells (Fig. 4C and D). In summary, we conclude that Pcl2 binds to *Hox* genes in a PRC2-dependent manner.

***Hox* repression by Pcl2 involves its functional interactions with PRC2 and PRC1.** We went on to test whether *Hox* repression by Pcl2 involves its interactions with PRC2. It is well established that Polycomb components cooperate to mediate *Hox* repression via physical interactions. Indeed, *Drosophila Pcl* was isolated as an enhancer for the *extra sex combs* (*esc*) mutation (33). Therefore, we examined the interactions between *Pcl2* and *Suz12* (an essential component of PRC2) mutant alleles. Since *Suz12* homozygous mutants die around 8.5 dpc, heterozygous embryos were used. Notably, even the heterozygous mutants exhibited homeotic transformations of the axis, albeit to a lesser extent than $Pcl2^{\Delta/\Delta}$ mutants (Fig. 5A and B) (21). The skeletal phenotypes were compared between $Pcl2^{\Delta/\Delta}$ and $Pcl2^{\Delta/\Delta}$; $Suz12^{+/-}$ mice at the newborn stage, and significant differences were identified around the cervicothoracic boundary. Anterior tuberculums, which are characteristic of the C6 vertebra, were associated instead with the C5 in $Pcl2^{\Delta/\Delta}$; $Suz12^{+/-}$. The C7 vertebrae were associated with perfect ribs, which were attached to the anteriorly shifted sternum.